Contrib Mineral Petrol (1989) 102:347–366

Contributions to Mineralogy and Petrology

Fluid and enthalpy production during regional metamorphism

James A.D. Connolly and Alan B. Thompson
Institute für Mineralogie und Petrographie, Eidgenossische Technische Hochschule, CH-8092 Zürich, Switzerland

Abstract. Models for regional metamorphism have been constructed to determine the thermal effects of reaction enthalpy and the amount of fluid generated by dehydration metamorphism. The model continental crust contains an average of 2.9 wt % water and dehydrates by a series of reactions between temperatures of 300 and 750° C. Large scale metamorphism is induced by instantaneous collision belt thickening events which double the crustal thickness to 70 km. After a 20 Ma time lag, erosion due to isostatic rebound restores the crust to its original thickness in 100 Ma. At crustal depths greater than 10 km, where most metamorphism takes place, fluid pressure is unlikely to deviate significantly from lithostatic pressure. This implies that lower crustal porosity can only be maintained if rock pores are filled by fluid. Therefore, porosities are primarily dependent on the rate of metamorphic fluid production or consumption and the crustal permeability. In the models, permeability is taken as a function of porosity; this permits estimation of both fluid fluxes and porosities during metamorphism. Metamorphic activity, as measured by net reaction enthalpy, can be categorized as endothermic or exothermic depending on whether prograde dehydration or retrograde hydration reactions predominate. The endothermic stage begins almost immediately after thickening, peaks at about 20 Ma, and ends after 40 to 55 Ma. During this period the maximum and average heat consumption by reactions are on the order $11.2 \cdot 10^{-14}$ W/cm^3 and $5.9 \cdot 10^{-14}$ W/cm^3, respectively. The maximum rates of prograde isograd advance decrease from $2.4 \cdot 10^{-8}$ cm/s, for low grade reactions at 7 Ma, to $7 \cdot 10^{-10}$ cm/s, for the highest grade reaction between 45 and 58 Ma. Endothermic cooling reduces the temperature variation in the metamorphic models by less than 7% (40 K); in comparison, the retrograde exothermic heating effect is negligible. Dehydration reactions are generally poor thermal buffers, but under certain conditions reactions may control temperature over depth and time intervals on the order of 1 km and 3 Ma. The model metamorphic events reduce the hydrate water content of the crust to values between 1.0 and 0.4 wt % and produce anhydrous lower crustal granulites up to 15 km in thickness. In the first 60 Ma of metamorphism, steady state fluid fluxes in the rocks overlying prograde reaction fronts are on the order of $5 \cdot 10^{-11}$ g/cm^2 – s. These fluid fluxes can be accommodated by low porosities (< 0.6%) and are thus essentially determined by the rate of devolitalization. The quantity of fluid which passes through the metamorphic column varies from 25000 g/cm^2, within 10 km of the base of the crust, to amounts as large as 240000 g/cm^2, in rocks initially at a depth of 30 km. Measured petrologic volumetric fluid-rock ratios generated by this fluid could be as high as 500 in a 1 m thick horizontal layer, but would decrease in inverse proportion of the thickness of the rock layer. Fluid advection causes local heating at rates of about $5.9 \cdot 10^{-14}$ W/cm^3 during prograde metamorphism and does not result in significant heating. The amount of silica which can be transported by the fluids is very sensitive to both the absolute temperature and the change in the geothermal gradient with depth. However, even under optimal conditions, the amount of silica precipitated by metamorphic fluids is small (< 0.1 vol %) and inadequate to explain the quartz veining observed in nature. These results are based on equilibrium models for fluid and heat transport that exclude the possibility of convective fluid recirculation. Such a model is likely to apply at depths greater than 10 km; therefore, it is concluded that large scale heat and silica transport by fluids is not extensive in the lower crust, despite large time-integrated fluid fluxes.

Offprint requests to: J.A.D. Connolly

Introduction

Much has been learned about the evolution of continental crust by combining the results of thermal modeling of the pressure(P) – temperature(T) – time(t) paths of regional metamorphism with observations on metamorphic rocks. The necessity for modeling arises because the large temporal and spatial scales of regional metamorphism make the P–T–t evolution of regional metamorphic systems difficult to evaluate from petrologic data alone. This paper presents the results of a computer model for the thermal budget of regional metamorphism and the evolution of metamorphic fluids. Previous studies have been based on models which take into account three major factors of regional metamorphic thermal budgets: (i) heat advection due to crustal thinning or thickening; (ii) variation in crustal heat flow; and (iii) changes in radioactive heat sources within the crust. However, only a few attempts have been made to model the effects of dehydration/hydration reactions on the thermal budget of regional metamorphism (Walther and Orville 1982; Ridley 1986; Peacock 1987, 1989) or to specifically consider the behavior and migration of such fluids

Table 1. List of symbols and some model constants

Symbol	Property	Units	Value
A	Radioactive heat production	W/cm^3	0 to $2 \cdot 10^{-12}$
C_f	Fluid head capacity	J/cm^3-K	3.7
C_r	Rock heat capacity	J/cm^3-K	2.5
D_p	Average grain size	cm	0.1
h	Heat	J	
H	Dehydration enthalpy	kJ/g_{H_2O}	-3.35 to 4.20
k	Permeability	cm^2	
K	Thermal conductivity	W/cm−K	$2.25 \cdot 10^{-8}$
K_o	Shape factor in the Carmen-Kozeny relation Eq. (3)		
P	Pressure	bar	
Q^*	Heat flux at base of lithosphere	W/cm^2	$3 \cdot 10^{-6}$
q_f	Fluid mass flux	g/cm^2-s	
t	Time	Ma or s	
T	Temperature	K or °C	
T_o	Fluid path tortuosity		
v_r	Erosional rock velocity	cm/s	0 to $-1.1 \cdot 10^{-9}$
z	Depth	km	
γ	Constant relating ϕ to q_f in Eq. (4)	g/cm^2-s	$-3.4 \cdot 10^{-4}$
ϕ	Rock porosity		
ρ_f	Fluid density	g/cm^3	0.95
ρ_r	Rock density	g/cm^3	2.80
μ_f	Fluid viscosity	g/cm−s	$1.5 \cdot 10^{-3}$
ω	Constant relating ϕ to k in Eq. (2)	cm^2	$2.9 \cdot 10^{-10}$

(Etheridge et al. 1983, 1984; Walther and Wood 1984; Wood and Walther 1986; Wall and Etheridge 1988)

In some previous investigations it has been concluded that the enthalpy associated with dehydration (Walther and Orville 1982) and hydration (Peacock 1987) reactions is significant and must be considered in thermal models. These conclusions were based on models which do not take into account the very substantial heat flow to the surface of the earth from crustal rocks during metamorphism. Thus, although these models provide useful constraints on the maximum importance of the enthalpy effect, they are probably too simplistic. The magnitude of the enhalpy effect was also considered, but not explicitly evaluated, by England and Thompson (1984, p 901), who suggested, in contrast to Walther and Orville (1982) and Peacock (1987), that the effect is a minor term in regional metamorphic thermal budgets. The arguments of England and Thompson are quite compelling, but despite this there are two reasons to incorporate dehydration/hydration reactions in metamorphic models. First, although the enthalpy effect is minor in comparison with the overall energy budget of metamorphism, metamorphic reactions may control local thermal states on short time scales (Fisher 1978; Ferry 1983, 1986; Ridley 1985). Modeling can reveal the scales over which such control may be operative, and also may provide insight into the way its effects could be preserved in metamorphic rocks. The second, and more important, reason is that dehydration/hydration reactions are the primary sources and consumers of regional metamorphic fluids at depths greater than 6–12 km. These fluids are of interest for many reasons, e.g.: (i) metamorphic fluids are often considered to be a transport medium for both heat and mass (e.g., Ferry 1986; Chamberlain and Rumble 1989a, b; Rumble 1988), the efficacy of fluid transport is, of course, critically dependent on fluid fluxes (e.g., Bickle and McKenzie 1987); (ii) the coincidence of fluids and certain $P-T$ conditions is necessary for retrograde hydration reactions (e.g., Fyfe et al. 1978) and, perhaps, crustal melting (e.g., Thompson 1988a); and (iii) the presence of pore fluids may have profound effects on the rheology and deformation styles observed in metamorphic rocks (e.g., Kirby 1984, 1985; Murrell 1985; Rutter and Brodie 1985; Rubie 1986; Thompson 1987, 1988b).

During regional metamorphism the locus and intensity of metamorphic activity varies both spatially and temporally within the crust. To describe these variations, models must take into account that metamorphic episodes are ephemeral, rocks may store fluids in pore space, and that the temperature, amount, and rates of dehydration/hydration will vary with depth. Such a model is developed here; this model combines simplified sub-models for metamorphic hydrology, reactions, and energy sources. The succeeding sections of this paper formulate each of these sub-models and present results from the integrated model. The reader should bear in mind that models presented are not intended to represent a specific metamorphic system, but rather, they are intended to illustrate the manner in which different metamorphic processes can be coupled, and to provide some limiting constraints on these processes. The symbols and constants used herein are summarized in Table 1.

Peacock (1989) has recently presented the results of a study very similar to that discussed here. The essential differences between the two studies are that here, retrograde hydration reactions, permeability constraints, mass transport (silica), and the development of metamorphic facies are considered.

Crustal hydrology

Metamorphic fluids are primarily composed of water which, for simplicity, will be assumed here to be the only volatile component of such fluids. This assumption has only minor consequences because the second most important

component of metamorphic fluids, carbon dioxide, has similar transport properties to water at elevated pressure (e.g., Walther and Orville 1982, p. 255). The upper and lower crust are characterized by drastically different hydrologic regimes determined by rock strength. In the upper crust, rocks have sufficient strength, on geologic time scales, to maintain networks of connected and underpressured pores. Consequently, fluid pressure in the upper crust tends to follow a hydrostatic gradient and is independent of lithostatic pressure. The independence of fluid pressure from lithostatic pressure is important for two reasons: (i) it is a necessary condition for downward fluid motion and, hence, for the development of convective fluid circulation cells; (ii) as long as fluid pressure follows a hydrostatic gradient, crustal fluids are mechanically stable, i.e., they have no tendency to migrate. The hydraulic conductivity of upper crustal rocks is quite variable and this variation is determined primarily by permeability. In situ measurements of upper crustal permeability have yielded values ranging from 10^{-9} to 10^{-16} cm^2 (e.g., Brace 1984).

Hydrology in the lower crust

In contrast to upper crustal rocks, rocks in the lower crust behave plastically on relatively short time scales so that porosity can only be maintained if rock pores are filled with a fluid at, or close to, lithostatic pressure. Lower crustal fluids, therefore, tend to follow a lithostatic pressure gradient. Under a lithostatic pressure gradient, fluids are inherently mechanically unstable and will always tend to migrate upwards. Thus, lower crustal fluids are ephemeral, and hydrologic systems in the lower crust must be regarded as "one-pass systems" (Walther and Orville 1982; Wood and Walther 1986; Valley 1986).

The boundary between the upper and lower crustal hydrologic regimes varies depending on rock competency, but, in general, the transition, which occurs over 2–3 km, takes place at depths of 6–10 km (Sibson 1983; Wood and Walther 1986; Fyfe et al. 1978). Given that crustal thicknesses are often in excess of 30 km, most regional metamorphism will occur in the lower parts and, therefore, the lower crustal hydrologic regime is an apt model for regional metamorphism. However, there are no direct measurements of permeabilities at lower crustal depths, so it is necessary to develop a model for permeability.

Lower crustal permeability

The porosity-permeability relations for crystalline materials are not well known, but on a theoretical basis it is predicted that permeability will be a power function of porosity. In this regard, the Carman-Konzeny relation:

$$k=[D_p^2/(36\,K_o\,T_o)]\phi^3/(1-\phi)^2, \tag{1}$$

which relates permeability (k) to the cube of porosity (ϕ), has been particularly useful for hydrologic problems (Bear 1979, p. 111, 166; Dullien 1979). In Eq. (1) D_p is the average grain size, K_o is a shape factor, and T_o is the tortuosity. For a given rock the term in the square brackets of Eq. (1) is thus a constant, ω. The terms composing ω have been defined differently by various authors, but for a rock with $D_p=0.1$ cm, estimates of ω range from $3\cdot10^{-5}$ to $9\cdot10^{-5}$ cm^2. These values yield permeabilities on the order of 10^{-11} cm^2 ($\phi=0.7\%$) which appear unacceptably high in view of the expectation that permeability is higher in the upper crust than in the lower crust (Brace 1984; Nehlig and Juteau 1988). As an alternative, ω was estimated by solving Eq. (1) given a porosity and permeability appropriate for a low permeability geologic material (i.e., the Westerly granite, $\phi=0.7\%$ and $k=10^{-16}$ cm^2, Trimmer 1982). This yields $\omega=2.9\cdot10^{-10}$ cm^2, which is assumed here to be valid for the $\phi-k$ relationship of lower crustal rocks in general. Noting that for most rocks $(1-\phi)^2$ is close to 1, Eq. (1) can thus be simplified to:

$$k\approx\omega\,\phi^3. \tag{2}$$

The minimum rock permeability, based on rates of grain boundary diffusion, was estimated by Walther and Orville (1982) to be on the order of 10^{-21} cm^2. This value is obtained for a porosity of 0.014% from Eq. (2). Thus, Eq. (2) yields reasonable permeability estimates for a wide range of porosities.

Lower crustal fluid fluxes

Because pore space in the lower crust can only be maintained if it is filled with a fluid phase which is near lithostatic pressure, rock porosity can be simply expressed as the fluid volume per rock volume. This fluid volume is determined by the amount of fluid generated, or consumed, by reactions and by the fluid fluxes into and out of the rock volume. Rates of reaction are determined by kinetic and thermal controls which will be discussed below, and fluid fluxes will be assumed to follow Darcy's law. Darcian fluid fluxes are related to the fluid pressure gradient ($\mathrm{d}P_f/\mathrm{d}z$) by the equation:

$$q_f=-k/\mu_f(\mathrm{d}P_f/\mathrm{d}z), \tag{3}$$

where μ_f is the fluid viscosity. For fluids subject to a lithostatic pressure gradient, ($\mathrm{d}P_f/\mathrm{d}z$) can be written $g(\rho_r-\rho_f)$; and, under most conditions of interest here, ρ_r, ρ_f, and μ_f can be treated as constants. Thus, Eq. (3) can be combined with Eq. (2) to obtain an expression for fluid fluxes in terms of porosity:

$$q_f=\gamma\phi^3. \tag{4}$$

Taking $\rho_r=2.8$ g/cm^3, $\rho_f=0.9$ g/cm^3, and $\mu_f=1.5\cdot10^{-3}$ g/cm$-$s (Walter and Orville 1982), the value for γ is $-3.4\cdot10^{-4}$ g/cm$^2-$s.

Equations (2) and (4) are developed on the basis of a model for porous media transport in which a discrete fluid phase migrates through a network of connected pores. However, in the lower crust it is possible that fluids may exist as grain boundary films, or that fluid motion is accomplished by migration of isolated fluid filled microcracks. The applicability of Eqs. (2) and (4) can therefore be questioned on a theoretical basis, and the assumption that these equations are valid as phenomenological laws is made here only as a first approximation. With this caveat, permeabilities and fluid fluxes calculated from Eqs. (2) and (4) for different porosities are summarized in Table 2. The fourth column of Table 2 contains the mass of fluid which would pass through a rock if the corresponding fluid flux in column three were maintained for 1 Ma.

An interesting feature shown in Table 2 is that, because fluid flux is a cubic function of porosity, small changes in porosity have a large effect on the efficiency of porous media transport. Large values of porosity, e.g. 2%, yield

Table 2. Permeability and fluid fluxes as a function of porosity

ϕ (%)	k(cm^2)	$-q_f$ (g/cm^2 − s)	Time-integrated flux after 1 Ma (g/cm^2)
2	$2\cdot10^{-15}$	$3\cdot10^{-9}$	85000
1	$3\cdot10^{-16}$	$3\cdot10^{-10}$	11000
0.5	$4\cdot10^{-17}$	$4\cdot10^{-11}$	1400
0.25	$5\cdot10^{-18}$	$5\cdot10^{-12}$	170
0.1	$3\cdot10^{-19}$	$3\cdot10^{-13}$	11
0.015	$1\cdot10^{-21}$	$1\cdot10^{-15}$	0.04

Table 4. Model pelite facies characteristics

Facies	Phase assemblage	Hydrate water content (wt %)
F_1	$H_1+H_2+H_3+H_4+H_5+H_6$	4.00
F_2	$A_1+H_2+H_3+H_4+H_5+H_6$	3.03
F_3	$A_1+A_2+H_3+H_4+H_5+H_6$	2.04
F_4	$A_1+A_2+A_3+H_4+H_5+H_6$	1.54
F_5	$A_1+A_2+A_3+A_4+H_5+H_6$	1.03
F_6	$A_1+A_2+A_3+A_4+A_5+H_6$	0.52
F_7	$A_1+A_2+A_3+A_4+A_5+A_6$	0.00

Table 3. Model pelite dehydration reaction characteristics

Reaction	T_{eq}(°C, $P=0$)	dT_{eq}/dP(°C/kb)	ΔH(kJ/g$_{H_2O}$)	Fraction of initial hydrate water released	Wt % H_2O bound in hydrate phase
$R_1(H_1=A_1)$	295	4.73	−3.22	0.25	8.0
$R_2(H_2=A_2)$	350	6.06	−3.22	0.25	8.0
$R_3(H_3=A_3)$	405	7.39	−3.44	0.125	4.0
$R_4(H_4=A_4)$	465	8.73	−3.66	0.125	4.0
$R_5(H_5=A_5)$	515	10.06	−3.88	0.125	4.0
$R_6(H_6=A_6)$	570	11.39	−4.10	0.125	4.0

permeabilities on the order obtained in upper crustal rocks and result in extremely high fluid fluxes. Such fluxes would rapidly exhaust a reservoir of free fluid. This efficiency deteriorates drastically with decreasing porosity, so that for a porosity of 0.015%, the fluid flux becomes negligible. The time-integrated fluid fluxes in Table 2, even for short time periods and low porosities, are large in comparison to what might be expected on the basis of petrologic fluid-rock ratios (e.g., Graham et al. 1983; Ferry 1986; Wood and Walther 1986). This discrepancy can be explained, at least partly, by the fact that petrologic fluid-rock ratios are invariably minimum values based on an estimate for the amount of chemical interaction between fluids and rock (Wood and Graham 1986). The fluid fluxes estimated in Table 2 are probably conservatively low, because large scale channeling of metamorphic fluids in fractures could increase rates of dewatering. Channeling, however, would decrease fluid-rock ratios on a petrographic scale because fluid in fractures will interact poorly with the adjacent rock matrix.

It is important to remember that Eq. (4) is valid only for fluids under lithostatic pressure; despite this it is also applied, in the modeling which follows, to the upper crust. This was done for simplicity and does not effect the modeling results in regions (depths greater than $\approx$12 km) where the assumption of a lithostatic gradient should be justified.

A petrogenetic grid for regional metamorphism

In theory is possible to develop a detailed thermodynamic model for the dehydration/hydration reactions of a specific lithology. However, given the heterogeneity of the crust, the goals of this study are served adequately by adopting an approximation of the pelite phase diagram. That the entire crust is composed of pelitic material is unlikely, but a pelite model is used here becauses it maximizes fluid generation. More plausible lithologies, e.g., amphibolites and gneisses, produce less fluid. A model based on pelite should therefore illustrate the maximum effects of dehydration/hydration reactions during metamorphism. The model used in this study is consistent with the following observations, premises, and assumptions: (i) Low grade pelites contain about 4 wt % water (Fyfe et al. 1978, p. 155). This value is taken to be representative of unmetamorphosed pelite. (ii) In comparison to high grade dehydration reactions, low grade dehydration reactions tend to release more water, be less endothermic, and have greater Clapeyron slopes. (iii) The enthalpy of low grade dehydration reactions (e.g., diaspore dehydration to corundum) is about −3.35 kJ/g H_2O. Whereas, for higher grade reactions (e.g., muscovite dehydration with quartz to aluminosilicate and potassium feldspar), the enthalpy approaches −4.2 kJ/g H_2O. The pressure dependence of reaction enthalpies is assumed to be negligible. (iv) Because of compositional variation (both in bulk composition and of individual minerals) the crust will dehydrate more or less continuously over a certain temperature interval. The lower and upper limits of this temperature interval are modeled after the diaspore and muscovite dehydration reactions, respectively. Thus, the model pelite will dehydrate from 300 to 550° C at a depth of 10 km (assuming and average rock density of 2.8 g/cm^3), and from 400 to 800° C at a depth of 70 km. The continuous pelite dehydration is modeled by a series of six discontinuous reactions R_1 through R_6, as described in Table 3. Each of these reactions involves the dehydration of a hypothetical hydrate, H_i, to its anhydrous equivalent, A_i, and free water. Given this petrogenetic grid (Table 3), there are seven equilibrium facies possible in model pelite crust, F_1 through F_7 as summarized in Table 4. Facies F_1 corresponds to essentially unmetamorphosed pelites, which contain 4 wt % water bound in hydrates H_1 through H_6, whereas facies F_7 corresponds to completely dehydrated pelite, i.e., granulite, which contains anhydrous phases A_1 through A_6. The hypothetical facies have water contents which are roughly similar to the average water contents of the major regional metamorphic facies, as estimated by Fyfe et al. (1978, p. 155).

Hydrates never coexist with their anhydrous equivalents in equilibrium facies (Table 4); however, because of free water loss and finite reaction rates, nonequilibrium facies

may occur. This is particularly important in the late stages of metamorphism when pervasive retrograde alteration can occur. Because much of this alteration would be nearly imperceptible, it is useful to define a second set of facies definitions to distinguish essentially equilibrium facies assemblages. For this purpose, "essentially equilibrium" facies are defined as a modification of equilibrium facies, in which the mode of one anhydrous phase is greater than 90% or less than 10% of its theoretical maximum and all other phases have modes equal to their theoretical maximum or minimum. Thus, the mineralogy of such a facies, designated F_i', is related to its equilibrium equivalent F_i by less than 10% alteration of one phase. Analytically, the "essentially equilibrium" facies F_i' is defined by the modal constraints: $\{A_{1-(i-2)}=0,\ A_{(i+1)-6}=100\%\}$, and $[\{A_{i-1}<10\%$ and $A_i=100\%\}$, or $[\{A_{i-1}=0$ and $A_i>=90\%\}]$ (constraints apply only when the indices are within the range 1 through 6).

Reaction rates

Ultimately the rates of metamorphic fluid production and consumption are determined by rates of metamorphic reactions. These rates, in turn, are determined by the rate of either heat input, mass transport, surface reaction mechanisms, or product nucleation, whichever is slowest (Lasaga 1986). Despite disparate models, the studies of Lasaga (1986), Walther and Wood (1984), and Ridley (1986), have all reached the conclusion that surface reaction mechanism and mass transport will be rate limiting only within a temperature range of a few Kelvins of the temperature at which product nucleation takes place. Inasmuch as the difference between the equilibrium temperature and the temperature of nucleation is expected to be small (Ridley 1986; Lasaga 1986), the true behaviour of a univariant metamorphic reaction is not appreciably different from the equilibrium model, given heat flow constraints. In view of this, it was decided not to incorporate models for reaction mechanisms and mass transport in the overall metamorphic model. This decision is further justified by the consideration that the exclusion of surface reaction mechanisms and mass transport presents the best case for rate control by heat flow and, therefore, the best case for thermal buffering by reactions.

Heat flow control of reaction rates is increasingly recognized as an important factor in both field (Ferry 1982; Fisher 1978) and theoretical studies (Ridley 1986; Ridley and Thompson 1986; Lasaga 1986). Such control arises because an endothermic dehydration reaction cannot consume an amount of energy greater than that which would result in cooling the rock, in which the reaction takes place, to the equilibrium temperature for the reaction. Likewise, exothermic hydration reactions cannot produce an amount of energy in excess of the amount of energy required to heat the rock above the equilibrium temperature. The amounts of energy which satisfy these constraints are primarily a function of the rate of heating or cooling that a volume of rock experiences. These rates are extremely variable and can be estimated by solving the relevant heat flow equations which are discussed later.

The physical and thermal model for crustal metamorphism

A number of mechanisms may cause regional metamorphism. In this study two crustal thickening mechanisms associated with orogeny are considered, homogeneous crustal thickening (vertical stretching-horizontal shortening) and crustal overthrusting. These mechanisms were selected over a mechanism such as whole lithospheric thickening because they produce larger thermal perturbations (England and Thompson 1984, 1986). Other mechanisms such as increasing lower-crustal heat flux, pervasive invasion of the lower-crust by mantle-derived melts, or crustal thinning may produce large scale thermal perturbations. However, they are not considered here because the time scales for these mechanisms are less easily constrained and because they occur subsequent to continental collisions when the crust has already been substantially dehydrated.

The size of the thermal perturbation associated with crustal thickening is dependent on a number of different factors which have been considered elsewhere (England and Richardson 1977; England and Thompson 1984, 1986). For reasons discussed by England and Thompson, a one-dimensional (vertical) model is considered here to be adequate to describe behaviour of average continental crust undergoing metamorphism. For present purposes the following "typical" configuration will be used as an illustration: (i) initial crustal and lithospheric thicknesses are 35 and 150 km respectively, (ii) the pre-thickened crust consists of an upper 15 km thick radioactive layer with radioactive heat production (A) equal to $2\cdot10^{-2}$ W/cm^3, and a lower nonradioactive layer, (iii) the average thermal conductivity (K), heat capacity (C_r), density (ρ) of the crust are, respectively, $2.25\cdot10^{-8}$ W/cm$-$K, 2.5 J/cm$^3-$K, and 2.8 g/cm^3, (iv) the heat flux at the base of lithosphere (Q^*) is $3\cdot10^{-6}$ W/cm^2 and the temperature at the surface of the crust is 273 K, (v) thickening occurs instantaneously and doubles the thickness of the crust to 70 km, (vi) there is a 20 Ma lag between the end of thickening and the onset of erosion, and (vii) erosion to isostatic equilibrium occurs in 100 Ma ($1.1\cdot10^{-9}$ cm/s). The effects of metamorphic reactions on the physical and thermal properties of the crust are assumed, as a first approximation, to be negligible. This configuration was chosen because it results in a large, but still geologically plausible, thermal perturbation from a typical continental geotherm. It should therefore permit estimation of the upper limits on the ability of metamorphic processes to generate fluids and regulate or influence heat flow.

To create optimum conditions for fluid generation it has been assumed that the water content at any depth in the crust is that of the equilibrium facies appropriate to the conditions of the initial geotherm. This implies crustal material accumulated at temperatures equal to or below those of the geotherm; any other case (previous metamorphism) would result in lower initial water content for the model. The equilibrium facies can be determined from the intersections of the steady state geotherm with the equilibrium curves for the dehydration reactions (Fig. 1a). This initial facies distribution results in an average crustal water content of 2.94 wt %. Although not explicitly demonstrated here, neither hotter nor colder geotherms generate more dehydration metamorphism. This is because models with hotter geotherms, which produce larger thermal perturbations (Thompson and England 1984), have as an initial condition a more anhydrous crust. Whereas, for cold geotherm models, which lead to more hydrous initial conditions, the thermal perturbation is smaller.

The geotherms and facies distributions in the crust im-

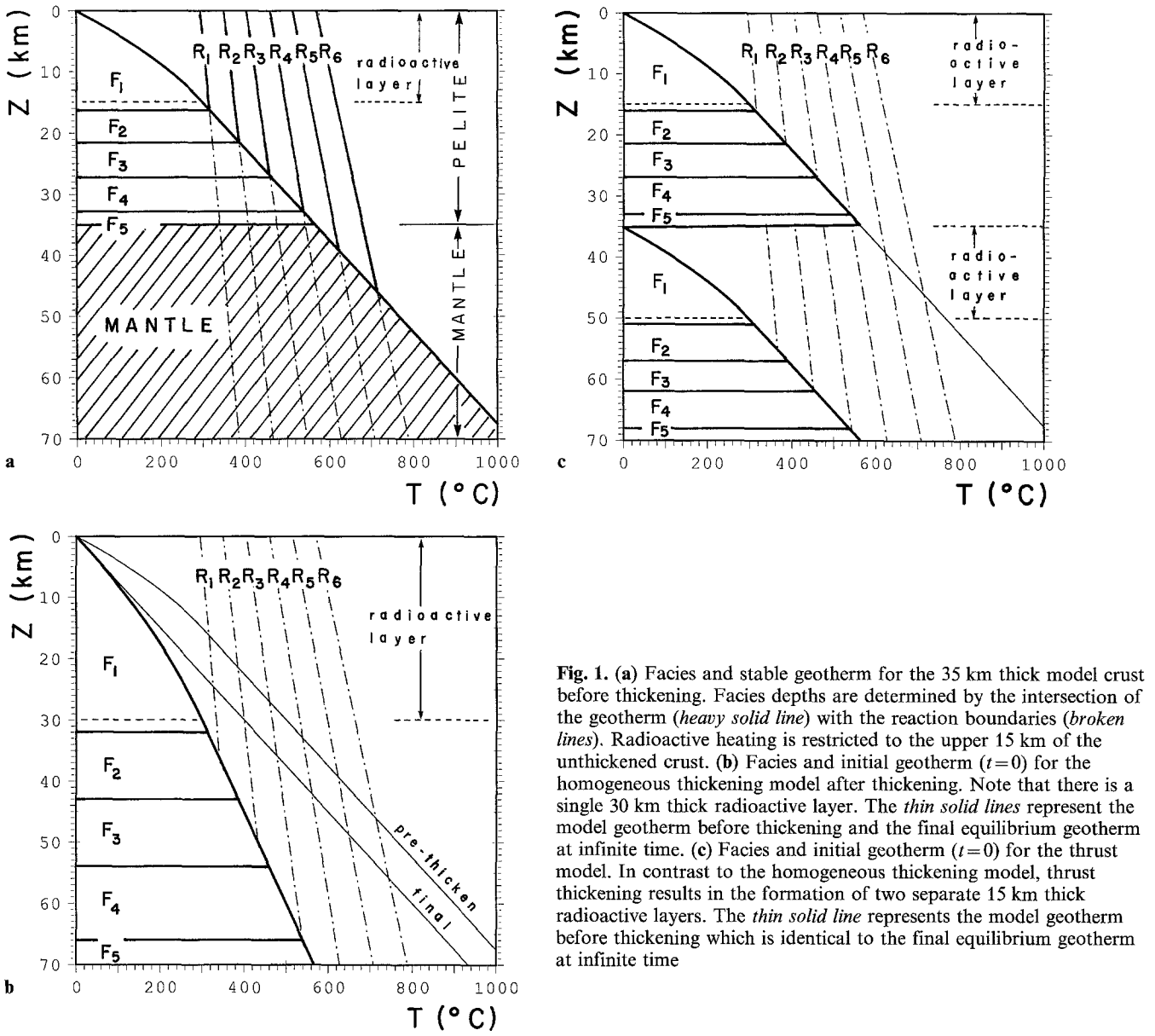

Fig. 1. (**a**) Facies and stable geotherm for the 35 km thick model crust before thickening. Facies depths are determined by the intersection of the geotherm (*heavy solid line*) with the reaction boundaries (*broken lines*). Radioactive heating is restricted to the upper 15 km of the unthickened crust. (**b**) Facies and initial geotherm ($t=0$) for the homogeneous thickening model after thickening. Note that there is a single 30 km thick radioactive layer. The *thin solid lines* represent the model geotherm before thickening and the final equilibrium geotherm at infinite time. (**c**) Facies and initial geotherm ($t=0$) for the thrust model. In contrast to the homogeneous thickening model, thrust thickening results in the formation of two separate 15 km thick radioactive layers. The *thin solid line* represents the model geotherm before thickening which is identical to the final equilibrium geotherm at infinite time

mediately ($t=0$) after homogeneous thickening and overthrusting are shown in Fig. 1. An important difference between the two models is that the thrust model superimposes hot less hydrous rocks over cool hydrated rocks. Thrusting, therefore, leads to an initial condition which is further from thermal and chemical equilibrium than is the initial condition for the homogeneous thickening model. Another distinction is that isostatic reequilibration will remove the upper radioactive portion of the crust (30 km) in the homogeneous thickening model; whereas, with the thrust model the final thickness of the radioactive layer is the same as the initial thickness (15 km). Consequently, the thrust model duplicates the initial unperturbed crustal conditions at equilibrium, but the homogeneous thickening model equilibrates to a cooler equilibrium geotherm (at infinite time).

Solution of the governing equations

The thermal evolution of the model crust after thickening is determined from the energy conservation equation:

$$\mathrm{d}h/\mathrm{d}t = K(\mathrm{d}^2T/\mathrm{d}z^2) + A + H - v_r C_r(\mathrm{d}T/\mathrm{d}z) - q_f'(\mathrm{d}T/\mathrm{d}z) - C_f T(\mathrm{d}q_f'/\mathrm{d}z) \quad (5)$$

which was solved by an implicit Crank-Nicholson finite difference approximation. The terms on the right in Eq. (5) represent, respectively, heat conduction, radioactive heat production, reaction enthalpy, heat advection by rock and fluid, and heat gain by addition of fluid mass. Equation (5) was solved assuming a fixed node spacing of 0.4625 km through the entire lithosphere and a variable number of nodes depending on the crustal thickness. Crustal compaction and densification in response to devolatilization was ignored. This can be justified by noting that the water bound in hydrates has a density of about 1.64 g/cm^3. Thus, the release of 3 wt % water in the crust would result in an increase of about 2.2% in the crustal density and a linear compaction of 1%, both of which are negligible compared to other sources of variability. The time step used in solving Eq. (5) was 0.1 Ma or, if less, one-fourth the time required to completely drain the fluid from the most rapidly draining node. The porosity associated with each

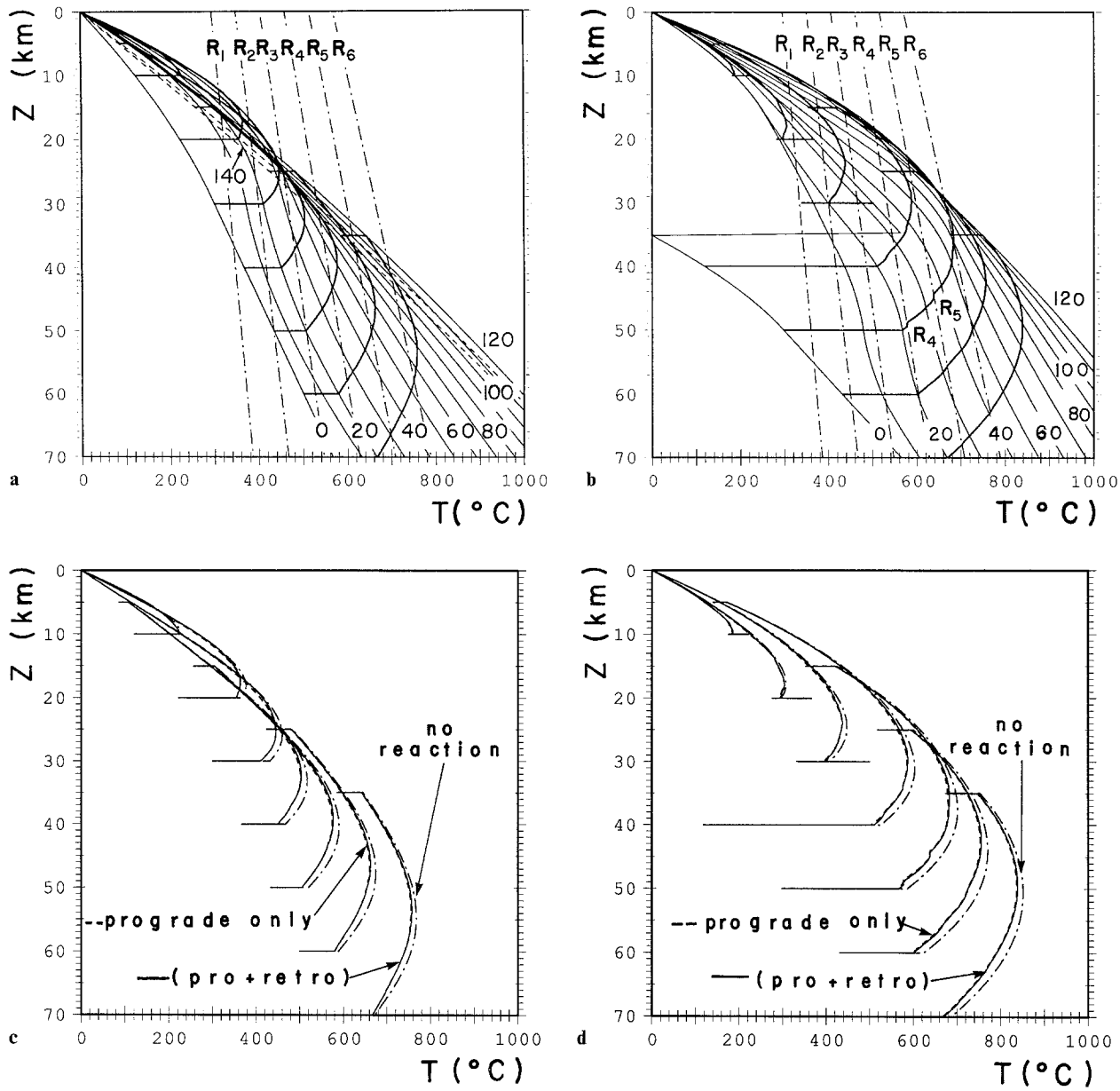

Fig. 2a–d. Geotherm evolution and $P-T-t$ paths for the homogeneous thickening (**a**) and thrust (**b**) models. Geotherms between 0 and 120 Ma are drawn as *thin solid lines* at 10 Ma intervals and labelled by the time in Ma. The geotherms at 130 and 140 Ma (after isostatic equilibrium) are drawn with *thin dashed lines* (**a**). $P-T-t$ paths are drawn as *heavy solid lines*. The R_1-R_6 reaction boundaries are shown by *broken lines*. The buffering effect of dehydration is apparent for the thrust model (**b**) when the $P-T-t$ path beginning at a depth of 50 km intersects the R_4 and R_5 reaction boundaries. $P-T-t$ paths for the homogeneous thickening (**c**) and thrust (**d**) models (*solid lines* labelled *pro+retro*) are compared to those for model variations without the effects of both dehydration and hydration (*broken lines* labelled *no reaction*) and without effects of hydration (*dashed lines* labelled *prograde only*)

node was calculated from the difference between the fluid fluxes into and out of the node plus internal production or consumption of fluid. The fluid flux into each node was computed from the porosity of the subjacent node with Eq. (4), and the flux out of a node by Eq. (4) and its own porosity. This approximation is a substantial simplification of the true fluid flow problem which has been treated by McKenzie (1985). The approximation leads to lower porosities and more rapid porosity diffusion, but is probably reasonable for the small compaction times and lengths estimated for the models. To facilitate calculations, the fluid was assumed to be pure incompressible water with a heat capacity (C_f) of 3.7 J/cm^3–K. Two final assumptions were made in solving Eq. (5); first, it was assumed that the bulk thermal conductivity was equivalent to the rock conductivity, and, second, the fluid flux q_f' was assumed to be equal to the Darcian fluid flux q_f relative to the rock reference frame. The first assumption is justified by the small proportion of free water expected in crustal rocks, and the second assumption is justified by the relatively slow erosional velocity of the crust. Mass and energy conservation constraints were evaluated to test the quality of the solutions to Eq. (5), in all cases both constraints were satisfied to within 98%.

The effect of reaction enthalpy on metamorphic temperatures

The evolution of the geotherms and $P-T-t$ paths for the homogeneous thickening and thrusting models are shown in Fig. 2a and b. An important difference between the two thickening models is that initial post-thickening temperature distribution for the homogeneous thickening model follows a normal geotherm, i.e., temperature increases continuously with depth and (d^2T/dz^2) is greater than or equal to zero. Thus, for the homogeneous thickening model, all $P-T-t$ paths are counter-clockwise in Fig. 2a which begins with a heating stage. In contrast, in the thrust model, the superposition of hot lower crustal rocks over cool upper crustal rocks results in a temperature inversion at the thrust plane. Rocks above the thrust plane therefore undergo substantial cooling in the first 10 Ma of the model evolution.

Basic differences in the thermal evolution of the models

Although by 10 Ma both models have roughly comparable temperatures (compare Fig. 2a and b), the subsequent evolution of the models differ because of the distribution of radioactive material. In the homogeneous thickening model, radioactive material occurs in a 30 km thick layer at the top of the post-thickened crust. This radioactive material is the primary cause of higher heating rates in the upper crust which causes the hot "bulge" in the early geotherms of the homogeneous thickening model. However, erosion gradually removes the radioactive portion of the crust (completely by 106 Ma) so that the radioactive heating effect diminishes with time. In the thrust model radioactive material occurs in the upper 15 km of both the autochthonous and allocthonous rock. Although the upper radioactive layer is removed by erosion, the lower layer remains throughout the evolution of the model. The radioactive heating effect associated with this layer (initially at a depth between 35 and 50 km) is especially strong because the layer is initially insulated from the surface boundary condition by the allocthnous rocks. The thrust model geotherms are therefore steeper and achieve temperatures more than 100 K higher in the homogenous thickening model.

The effect of reaction enthalpy on the shape of $P-T-t$ paths

The $P-T-t$ paths in Fig. 2 illustrate that the effect of reaction enthalpy has only minor influence on the typical counter-clockwise shaped $P-T-t$ path. The influence is most apparent for the thrust model (Fig. 2b) where it can be seen that the $P-T-t$ paths are constrained to follow the equilibrium conditions for dehydration reactions for short time and depth intervals. For example, the $P-T-t$ path which follows the evolution of rocks at an initial depth of 50 km, follows the equilibrium conditions of reactions R_4 and R_5 for depth intervals of about 1 km or a time period of 2.8 Ma. The influence of dehydration reactions on the $P-T-t$ paths for the crustal homogeneous thickening model is almost imperceptible because the geotherms intersect the reaction curves at a higher angle than in the thrust model.

The effect of reaction enthalpy on T_{max}

The influence of reactions which take place during the 20 Ma interval between thickening and the onset of erosion cannot be seen in Fig. 2a and b, but can be observed if the $P-T-t$ paths are compared to those obtained when no reactions occur, as shown in Fig. 2c and d. This comparison of $P-T-t$ paths reveals that the net effect of reaction enthalpy is to reduce the maximum temperatures (T_{max}) achieved during metamorphism by about 35 K, which, in view of the total temperature variation, is not particularly significant. Reaction enthalpies do not effect the timing or depth at which T_{max} is reached in any significant or systematic way.

The retrograde enthalpy effect

The $P-T-t$ paths shown in Fig. 2a and b take into account both endothermic prograde dehydration reactions and exothermic retrograde hydration reactions. Because the models assume a porous media fluid flow, which is the least efficient means of fluid transport, the maximum amount of fluid is available for retrograde hydration reactions and therefore the models demonstrate the maximum exothermic effect. If instead, fluid were to escape rapidly through fracture systems no exothermic retrograde hydration effect would be observed. The dashed $P-T-t$ paths in Fig. 2c and d illustrate this case. Comparison of the $P-T-t$ paths in Fig. 2c and d calculated with and without hydration reactions demonstrate that retrograde exothermic hydration raises crustal temperatures by less than a few Kelvins.

Distribution of facies and water during metamorphism

The interpretation of the thrust model is somewhat complicated because the initial post-thickening facies distribution metamorphic grade does not increase continuously with depth. For this reason, it is easier to consider only the interpretation of the homogeneous thickening model first (Figs. 1a and 2a). Because of the conclusions drawn from the homogeneous thickening model apply, at least qualitatively, for the thrust model, the discussion of the thrust model at the end of this section addresses only major differences between the models.

Results from homogeneous thickening model

Evolution of metamorphic facies. The variation in the depth of facies with time during metamorphism for the homogeneous thickening model is shown in Fig. 3. Each facies boundary in Fig. 3 would be recognized in natural rock exposures as the isograds corresponding to reactions R_1 through R_6 with increasing depth. The facies boundaries may be equilibrium or nonequilibrium. They are equilibrium boundaries if the depth-time coordinates of the isograd (Fig. 3) coincide with the depth-time coordinates of the isograd reaction curve and crustal geotherm in Fig. 2a. Immediately after thickening (time = 0 in Fig. 3) all facies are metastable with respect to more hydrous, lower grade, assemblages. However, because the model crust intially has essentially no free water phase, retrograde hydration cannot occur and the first reaction to occur must necessarily be prograde dehydration. The facies boundaries come into equilibrium at the points labelled (i) in Fig. 3, which correspond to the beginning of prograde dehydration. Each of the isograds then remain in equilibrium until the point labelled (iv), as can be verified from Fig. 1a. The generally

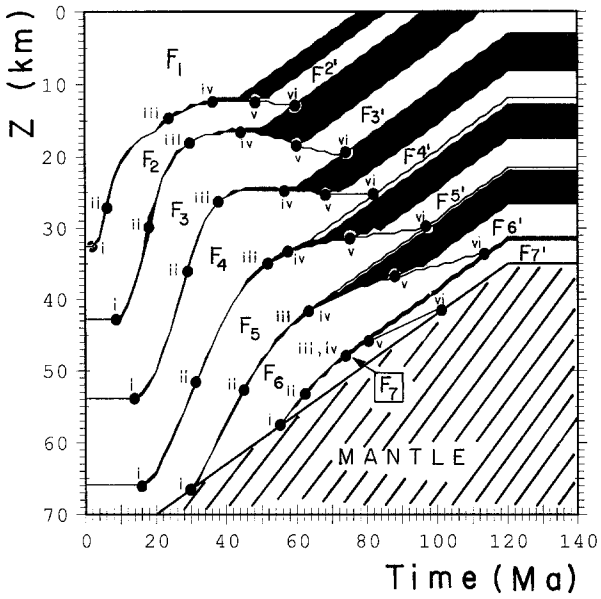

Fig. 3. Facies development as a function of time for the homogeneous crustal thickening model (Figs. 1b and 2a). Line widths reflect the actual width of facies boundaries. The position of the base of the crust is indicated by the *heavy solid line*. Labelled points along the facies boundaries correspond to: (*i*) Time at which a facies boundary first corresponds to a prograde reaction front. (*ii*) Time at which prograde reaction front reaches it maximum upward velocity. (*iii*) Time at which reaction front changes from prograde to retrograde. (*iv*) Time at which complete retrograde equilibration ceases. (*v*) Time beyond which a retrograde reaction converts less than 10% of its anhydrous reactant to hydrate. (*vi*) Time at which the retrograde front becomes completely inactive. Slight irregularities in the facies boundaries occur because continuous thinning of the crust by erosion is simulated by discrete steps of 0.4625 km at intervals of 1.32 Ma

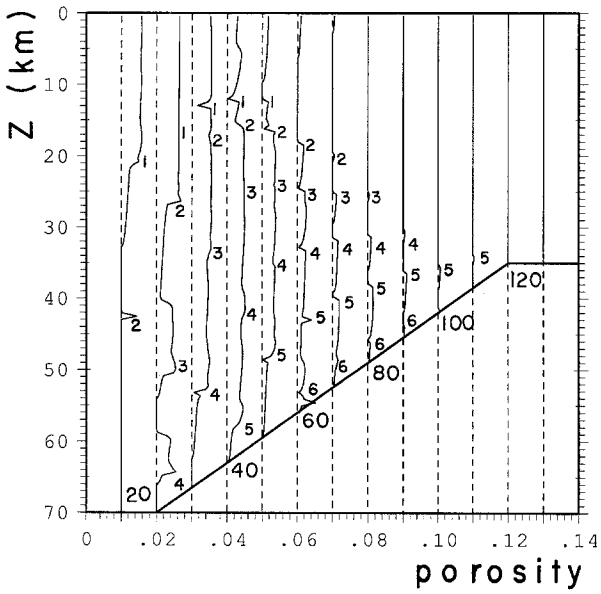

Fig. 4. Crustal porosity profiles at 10 Ma year intervals from 0 to 140 Ma for the homogeneous crustal thickening model. The zero baseline for each profile is shifted by 0.01 porosity units for every 10 Ma of model time. Alternate profiles are labelled by time in Ma and position of the base of the crust is indicated by a heavy solid line. Position of active reaction fronts, determined from Fig. 3, are indicated by the reaction numbers

narrow width of facies boundaries, during the time period between points (i) and (iii), reflects the fact that the isograd reaction rates are controlled by the metamorphic heat flux. However, several time periods in which low heat fluxes permit reaction control of the local thermal state are evident from widening of the isograds (Fig. 3). The most notable of these periods occurs in the first 20 Ma of metamorphism, before the onset of uplifting, and therefore is not apparent in the $P-T-t$ paths of Fig. 2a or c.

Rates of isograd advance. The rate of prograde advance of reaction isograds through the crust is given by the slope of the curves which trace the depth-time coordinates of the isograds (Fig. 3) less the uplift rate. The depth-time coordinate at which this rate reaches a maximum is identified for each isograd in Fig. 3 as point (ii). For the R_1 and R_2 isograds the maximum rates of advance are $6.6 \cdot 10^{-9}$ and $7.3 \cdot 10^{-9}$ cm/s, respectively; the maximum rates then decrease progressively with grade to a low of $0.85 \cdot 10^{-9}$ cm/s for the R_6 isograd. Criteria for determining the period of peak prograde metamorphic activity are somewhat arbitrary, but this period must fall within the time interval over which maximum rates of isograd advance occur. For the homogeneous thickening model, this interval occurs between 6 and 63 Ma. Points labelled (iii) in Fig. 3 (at which the slope of the curves which trace the depth-time coordinates of the facies boundaries first becomes parallel to the depth-time trajectory of the base of the crust) indicate the time and depth at which isograds cease upward prograde movement and begin to move downward through retrograde hydration. Because this point occurs progressively later with increasing grade, lower grade isograds $R_1 - R_3$ begin retrograde motion before the peak rates of prograde activity for isograds R_5 and R_6.

Fluid production and porosity during prograde metamorphism. The amount of free water present in the crustal rocks can be measured in terms of porosity because of the model assumptions that water has constant density, 0.9 g/cm^3, and that rock porosity can be maintained only when pores are filled by water. The distribution of free water, as measured by porosity, with depth in the crust for the homogeneous thickening model is shown in Fig. 4 at 10 Ma intervals. To make Fig. 4 legible, the 0 porosity baseline for each depth vs. porosity profile is incremented by 0.01 units for every 10 Ma of model time. Thus, porosities at 10 Ma are measured relative to the 0.01 ordinate on the porosity scale, and at 100 Ma they are measured relative to the 0.1 ordinate.

The crustal porosity profiles in Fig. 4 show that by 10 Ma water produced by reaction R_1 has reached the surface and that the resultant average crustal porosity, above the reaction front (20.3 km, from Fig. 3), is on the order of 0.5%. Because fluid is only produced near the reaction front, porosity gradually decreases below the front, reaching zero at 32.5 km, the depth at which R_1 isograd first became active. The small spike in the porosity profile at 42.6 km is due to the beginning of the dehydration reaction R_2. By 20 Ma three separate regions of high porosity have developed; each of these is related to a isograd reaction front which can be identified as the R_2, R_3, and R_4 reactions at depths of 25.8, 49,7, and 64.0 km, respectively (Fig. 3).

The porosity profile associated with an individual pro-

grade reaction has a characteristic form. This consists of a small peak associated with the reaction front below a region of near uniform high porosity and above a region in which porosity decreases reaching zero immediately below the initial depth of the reaction front. The form of the profiles result because when fluid is first produced rock permeability is too low to allow the fluid to leave as rapidly as it is produced. Once the porosity reaches a value that permits a fluid flux comparable to the rate of fluid production, porosity cannot increase further and changes only with variation in the rate of advance of prograde isograds. Because fluid flux is proportional to the cube of porosity [Eq. (4)], a variation of three orders of magnitude in the rate of isograd advance is required to produce an order of magnitude variation in porosity. However, as can be seen in Fig. 3, the rate of isograd advance is not particularly variable, hence the nearly constant porosities above reaction fronts during prograde metamorphism (Fig. 4). Below prograde reaction fronts the porosity decreases abruptly within less than 1 km such that permeabilities reach a value low enough that pore water fluxes become negligible. Thus, the fluid flux above the reaction fronts in the 20 Ma profile in Fig. 4 can be associated with individual reactions. For the observed porosities which range from 0.4 to 0.6%, the corresponding reaction generated fluid fluxes, from Eq. (4), are between $2 \cdot 10^{-11}$ and $7 \cdot 10^{-11}$ g/cm^2 – s. At later model times the contribution of individual prograde reactions to the metamorphic fluid flux is largely obscured by mixing of fluids generated by more than one reaction.

Retrograde fluid consumption and facies modification. The first retrograde activity in the homogeneous thickening model begins at 24 Ma when the R_1 isograd begins moving downward relative to the base of the crust (point (iii) on the F_1 and F_2 facies boundary in Fig. 3). The evidence of this retrograde activity in the porosity profile at 30 Ma (Fig. 4) is an abrupt porosity decrease in the vicinity of the R_1 reaction front (13 km in Figs. 4 and 3). Eventually, accelerated cooling in the upper crust, in conjunction with waning prograde activity at depth, permits retrograde hydration to consume the entire metamorphic fluid flux. Thereafter, retrograde fronts descend (see below) leaving dry partially equilibrated rocks in their wake. The point at which this occurs for each reaction is identified as point (iv) in Fig. 3. By 40 Ma, rocks on the reaction front are completely dry and a significant reduction in crustal porosity occurs above the reaction front. These features indicate that retrograde hydration of facies F_2 is consuming the fluid flux generated by prograde activity at greater depths. Eventually, as prograde activity wanes, the retrograde fronts descend leaving dry partially equilibrated rocks in their wake. Thus, by 50 Ma there is a dry region between 9.5 km and the R_1 reaction front at 12 km.

The depth at which retrograde reaction fronts become active (points (iii) in Fig. 3) increases with time. Thus, at the onset of the first retrograde metamorphism at 24 Ma the entire metamorphic fluid flux is available to supply the R_1 hydration reaction front. However, activation of the R_2 hydration reaction front at 30 Ma gradually reduces the flux into the overlying rocks until it is completely cut off by 45 Ma (point (iv) on the R_2 isograd in Fig. 3). Once this occurs, the only fluid available to the R_1 front is the pore water between the R_1 and R_2 fronts at 12.2 and 16.2 km. While a component of this water migrates upwards, the power law relationship between porosity and permeability precludes the possibility of complete drying by upward fluid flow. Thus, inevitably the R_1 front will descend until it encounters rocks which have been dried, and therefore only partially equilibrated, by the R_2 front (point (vi) at 13 Km and 59 Ma in Fig. 3). Similar constraints operate for each retrograde front, with the end result that by the end of retrograde activity (at 113 Ma) no pure facies assemblages persist, i.e., all assemblages contain an anhydrous phase which has been partially converted to its hydrous equivalent. However, a substantial proportion of the crust retains "essentially equilibrium" assemblages, i.e., the extent of the hydration reaction is negligible (<10%) or essentially complete (<90%). In these regions the assemblages can be classified as the modified facies F'_1 – F'_7 described earlier. The amount of retrograde alteration varies more or less continuously, therefore, each of these facies is separated in depth by an interval (filled in Fig. 3) in which an anhydrous phase has undergone more than 10% alteration.

In comparison to the upward velocity of prograde isograds, the downward velocity of retrograde isograds is quite slow. In the time interval between points (iii) and (iv), during which complete hydration occurs, downward isograd velocities are always less than 10^{-9} cm/s. Because these velocities are on the same order as the erosional velocity, the slight thickening of the isograds reflects limitations of the finite difference algorithm and cannot be interpreted as thermal buffering. Nonetheless, the position of the geotherm relative to the reaction boundaries in Fig. 2a confirms that the position of retrograde reaction fronts, points (iii–vi) in Fig. 3, is determined by the rate of cooling. Beyond point (iv), however, the metamorphic fluid fluxes are too low to permit complete equilibration. An interesting counterintuitive implication of this is that rocks which cool slowly could retain sharper (less altered) facies transitions than rocks which cool rapidly.

Effect of fluid channelling on facies distributions. Because of low metamorphic porosities, complete retrograde hydration occurs only when fluid fluxes are high (e.g., for reactions R_1 through R_3 during the time intervals between points iii and iv in Fig. 3). Once these fluxes diminish, the amount of retrograde hydration is primarily controlled by the amount of in situ free water. As noted earlier, the porous media fluid transport model employed here represents the least efficient transport model and, therefore, maximizes in situ water and the retrograde effect. If metamorphic fluids were removed more efficiently by fracture flow, then little, if any, retrograde metamorphism would occur. This limiting case was simulated by excluding the possibility of retrograde hydration in the model and the resulting facies distributions are shown in Fig. 5. Comparison of Figs. 3 and 5 demonstrates that the most notable effects of retrograde metamorphism is to obscure facies transitions and to result in lower grade rocks being exposed at the surface.

Differences between homogenous thickening and thrust thickening

Hydration reactions do not occur in the initial stages of the homogeneous thickening model because the first prograde activity occurs in the upper portion of the crust and moves downward with time. In the early stages of the thrust

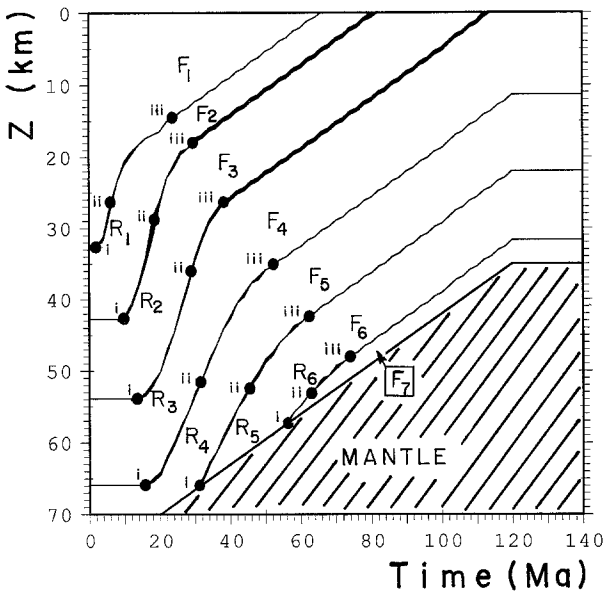

Fig. 5. Facies development as a function of time for the homogeneous crustal thickening model without hydration reactions. Labelling as described for Fig. 3

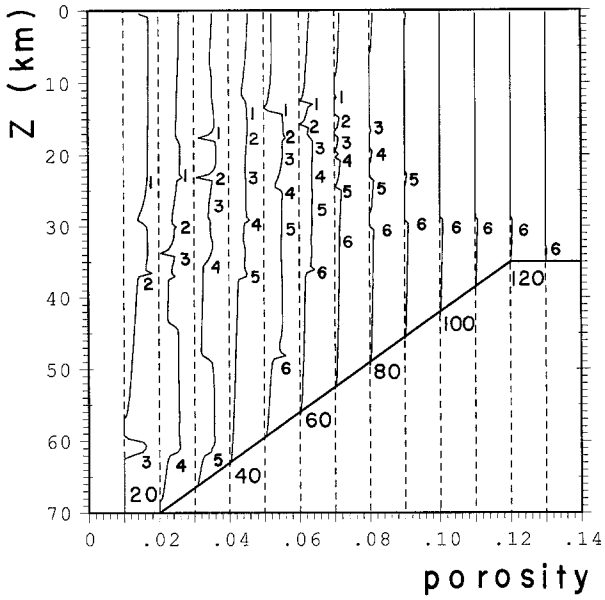

Fig. 7. Crustal porosity profiles for the thrust thickening model as described for Fig. 4. Positions of reaction fronts determined from Fig. 6

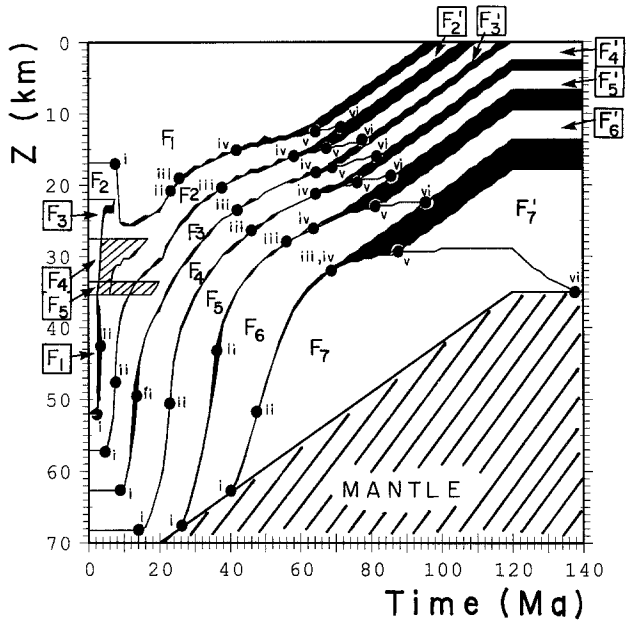

Fig. 6. Facies development as a function of time for the thrust thickening model. Labelling as described for Fig. 3. Rocks in the small hatched region for model times from 2 Ma to 14 Ma have phase assemblages which cannot be categorized as one of the seven hypothetical facies

model, upper crustal rocks cool, consequently these rocks undergo extensive retrograde hydration once they are permeated with the fluids generated by the dehydration of underlying crustal rocks. From Fig. 6 it can be seen that in the thrust model the first fluids are generated rapidly and in large quantities when facies F_1 rocks between 35 and 51.5 km are heated through the R_2 isograd (Fig. 6) in the time interval 2.3–3.0 Ma. These fluids reach the cold allochthonous facies rocks by 2.4 Ma, and by 7 Ma have driven the retrograde reaction R_2 to completion from 35 to 20 km. Retrograde reactions R_3 and R_4 do not occur initially in the upper facies F_4 and F_5 rocks because the rocks have already cooled below the kinetic blocking temperatures (assumed to be 100 K below the equilibrium temperatures) by the time the fluids first reach them. Consequently, a small region of the crust (the hatched region of Fig. 6) does not completely equilibrate until 19 Ma, at which point a normal equilibrium facies series obtains. Thereafter, the features of the thrust model (Fig. 6) are similar to those of the homogeneous thickening model (Fig. 3) and may be interpreted identically.

Maximum rates of prograde isograd advance are greater in the thrust model (points ii in Fig. 6 correspond to rates between $32 \cdot 10^{-9}$ and $4.0 \cdot 10^{-9}$ cm/s for isograds R_2 through R_6) than they are in the homogeneous thickening model. These high rates, particularly for the $R_1 - R_3$ isograds in the autochthon, partially reflect the initial geotherm of the thrust model. The large temperature contrast of this geotherm exaggerates rates of heating and, thus, metamorphism in the early stages of the model. However, based on more accurate modelling of thrust thickening (e.g., Shi and Wang 1987), the temperature inversion and high heating rates of the thrust model are at least qualitatively correct. More generally, large isograd velocities in the thrust model reflect the fact that the geotherms are steeper and more nearly parallel to the Clapeyron slopes of the isograd reactions in the depth region where most metamorphism takes place. Thus, a small uniform increase in the geotherm temperatures causes a large shift upwards in the equilibrium depth of the isograd. This shift is maximized as the slope of the geotherm approaches the slope of the isograd reaction boundary. The high rate of prograde metamorphism in the thrust model is reflected by high porosities (Fig. 7) which are often in excess of 0.6%. Because the thrust model cools to a hotter steady state geotherm than does the homogeneous thickening model, retrograde metamorphism begins later and proceeds more slowly in the thrust model.

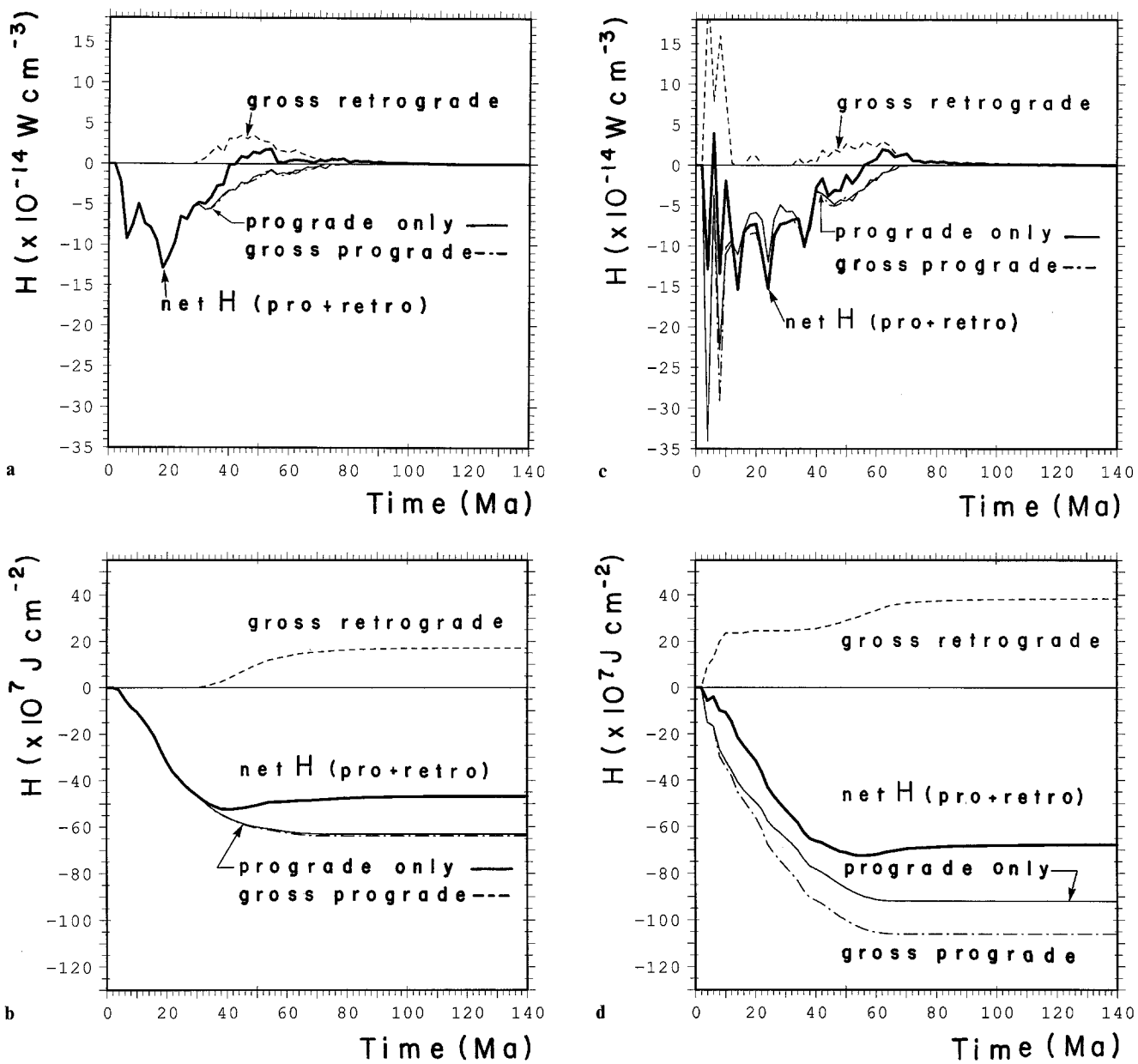

Fig. 8a–d. Instantaneous and time-integrated enthalpy terms are plotted in **a** and **b**, respectively, for the homogeneous thickening model and in **c** and **d**, respectively, for the thrust model. The *heavy solid, thin dashed*, and *thin broken curves* represent net (*prograde + retrograde*), gross exothermic (*retrograde*), and gross endothermic (*prograde*) model enthalpies. The *thin solid curves* represent the enthalpy for the models without hydration reactions (*prograde only*)

Reaction heat in the metamorphic heat budget

The cumulative and instantaneous amounts of reaction heat consumed or produced in the two metamorphic models are shown in Fig. 8. In considering Fig. 8, it should be noted that instantaneous enthalpy production (Fig. 8a and b) is expressed per unit volume, whereas the cumulative enthalpy production curves (Fig. 8c and d) represent the enthalpy produced in a cm^2 column of crust. Because the crustal thickness varies from 70 km at 20 Ma to 35 km by 120 Ma, this means that a fixed amount of dehydration in the crust produces the same effect on the cumulative curves of Fig. 8 regardless of the time; but, can results in a larger effect in the instantaneous curves if it occurs later in the model evolution. Consequently, the instantaneous enthalpy production curves are not exact derivatives of the cumulative curves.

Temporal variation in reaction heat after homogeneous thickening

The major stages in the metamorphic episode generated for the homogeneous thickening model are easily identified in Fig. 8a and b. During the prograde stage, net heat consumption by dehydration reactions reaches a maximum of $1.3 \cdot 10^{-13}$ W/cm^3 at 18 Ma; heat consumption then decreases, reaching zero at 41 Ma (Fig. 8a). This point, which corresponds approximately to the minimum in the cumulative net enthalpy curve of Fig. 8b, is the point at which the net effect of reaction enthalpy in the crust changes from cooling to heating. Because hydration is exothermic and dehydration is endothermic, this point can also be considered to represent the transition from the prograde to retrograde stages of metamorphism. The maximum in net retrograde heat production, which occurs at 54 Ma (Fig. 8a),

is about $1.8 \cdot 10^{-14}$ W/cm^3, an order of magnitude less than the maximum net prograde heat consumption. That the maximum gross retrograde heating occurs at 44 Ma, 10 Ma earlier than the maximum net heating, demonstrates that a requisite for extensive retrograde activity is prograde fluid release at depth. From the cumulative heat production curves in Fig. 8b, it can be seen that although the gross retrograde effect, $1.7 \cdot 10^8$ J/cm^2, is roughly one-fourth of the gross prograde enthalpy effect, $6.4 \cdot 10^8$ J/cm^2; the net retrograde effect, $6 \cdot 10^7$ J/cm^2, is negligible in comparison to the net prograde cooling effect, $5.2 \cdot 10^8$ J/cm^2. An interesting feature of Fig. 8b is that the enthalpy for the model without retrograde hydration reactions is slightly less than the gross endothermic enthalpy for the normal model. The explanation for this is that retrograde heating results in slightly hotter $P-T-t$ paths which permit more dehydration to take place.

Temporal variation in reaction heat after thrust thickening

In comparison to homogeneous thickening, in the thrust model the production and consumption of reaction heat varies much more irregularly (Fig. 8c). This again reflects the fact that in the thrust model the geotherms are often nearly parallel to reaction boundaries (Fig. 8c). Thus, reaction activity occurs in large pulses when the geotherms coincide with the conditions for a reaction. Although taken separately the cumulative gross endothermic and exothermic reaction enthalpies generated in the thrust model (Fig. 8d) are nearly twice as large as for the homogeneous thickening model, the net heat consumption is only slightly greater ($6.7 \cdot 10^8$ W/cm^2) for the thrust model. Because of the large pulses in retrograde hydration early in the thrust model, the maximum rates of net enthalpy consumption, around $1.5 \cdot 10^{-13}$ W/cm^3 at 14 and 24 Ma, occur considerably later than the maxima in the gross endothermic enthalpy. The rates of net heat consumption and production are comparable for both models, but the timing for the last retrograde stage of metamorphism is somewhat different. In the thrust model, the transition from prograde cooling to retrograde heating occurs at 56 Ma and the peak in retrograde heating at 62 Ma, 12 and 8 Ma later than in the homogeneous thickening model. The difference between the endothermic enthalpy curves for the thrust model with and without hydration reactions is larger than in the homogeneous thickening model because the initial retrograde activity in the thrust model generates hydrates which are subsequently dehydrated.

Reaction heat in comparison to other thermal factors

Some feeling for the magnitude of the reaction heat in terms of the overall metamorphic thermal budget can be obtained by calculating the time averaged enthalpy production during prograde metamorphism. For the homogeneous thickening model, the prograde stage is 36 Ma long during which the average crustal thickness is 68.06 km and $5.2 \cdot 10^8$ J of heat are consumed per cm^2 of crust, with these values the average (net) heat consumption is $6.1 \cdot 10^{-14}$ W/cm^3. In the thrust model $5.2 \cdot 10^8$ J/cm^2 are consumed over a time period of 54 Ma while the average crustal thickness is 65.8 Km. Thus, the average heat consumption is $6.5 \cdot 10^{-14}$ W/cm^3, virtually the same as in the homogeneous thickening model. These average values are about half the maximum rate of heat consumption, $1.3 \cdot 10^{-7}$ W/cm^3. For comparison, during erosion the rock advection term in Eq. (5) is on the order of $4.2 \cdot 10^{-13}$ W/cm^3 (for a 20 K/km geothermal gradient) and the radioactive heating term in Eq. (5) is $2.1 \cdot 10^{-12}$ W/cm^3 for radioactive rocks. The heat consumption during the endothermic stage of the homogeneous thickening model would be compensated by a heat flux of approximately 0.1 HFU, whereas the total variation in surface heat flow is 1 HFU ($4.2 \cdot 10^{13}$ W/cm^2) for the model. Heat consumed during the endothermic stages of metamorphism is thus, as best, only marginally significant in the overall metamorphic thermal budget. Inasmuch as the heat produced during the exothermic stage of metamorphism is about one tenth of the heat consumed during the endothermic stage, the exothermic effect is negligible.

Fluid fluxes and heat and mass transport by fluid advection

Through Eq. (4), Figs. 4 and 7, which show crustal porosity as a function of time, can be used to determine the instantaneous fluid fluxes for the crustal models at any time and depth. These fluxes integrated through time are plotted in Fig. 9. For each model, the time-integrated fluid flux is shown for rocks at initial depths at 10 km intervals from 10 to 60 km (solid curves); in addition, the time-integrated surface fluid flux is also plotted (dashed curve). In the absence of retrograde metamorphism, time-integrated fluxes in a static metamorphic column should increase upwards because all free water passes through the overlying rocks and is ultimately expelled at the earths surface (or at least above the depth of the lithostatic-hydrostatic fluid pressure transition). This simple pattern is not observed in the models used here both because of retrograde resorbtion of fluids and because erosion removes a significant portion of the crust simultaneously with metamorphism. In both models time-integrated fluxes therefore reach maxima in rocks of which the initial depths were around 20–30 km. However, because rocks above initial depths of 35 km are removed by erosion, the final time-integrated fluxes follow an upward increasing pattern. For rocks at initial depths from 60 to 30 km, the time-integrated fluxes increase from 25000 to 240000 in the thrust model; these fluxes are almost three times greater than those calculated for the homogeneous thickening model. This difference between the models reflects the facts that the lower 35 km of crust in the thrust model initially contains more hydrate water (2.92 wt % as opposed to 1.94 wt %) and is more anhydrous by the end of metamorphism (0.40 wt % as opposed to 1.04 wt %) than the homogeneously thickened crust.

Measured fluid-rock ratios

In studies of natural metamorphic rocks, the fluid-rock ratios estimated from isotopic or petrologic data are typically on the order of 0.1–20, though recently ratios of up to 10000 have been estimated in mineralized fractures (Rumble 1988). It is very important to realize that measured ratios are only indirectly related to the fluid fluxes estimated by modelling.[1] This is deduced by noting that ideally petrologic fluid-rock ratios, F, are measured from a phase assemblage uniformly distributed over a section of rock with di-

[1] The authors are grateful to Mike Bickle for pointing out the error of equating time-integrated fluid fluxes with fluid-rock ratios.

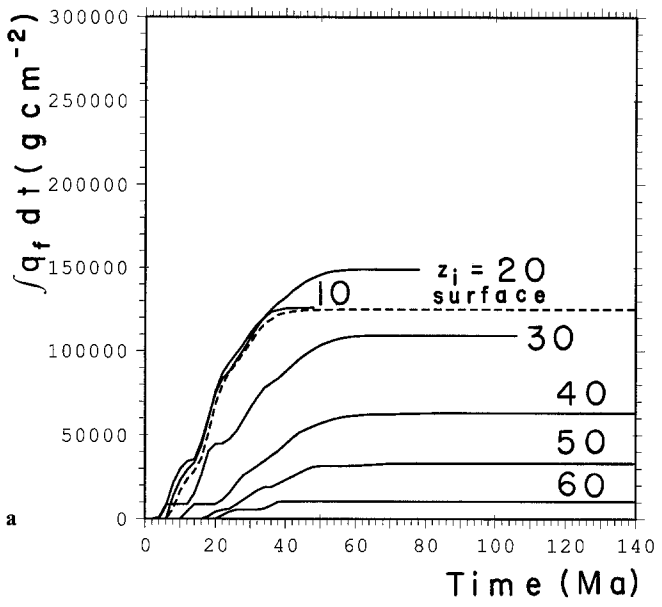

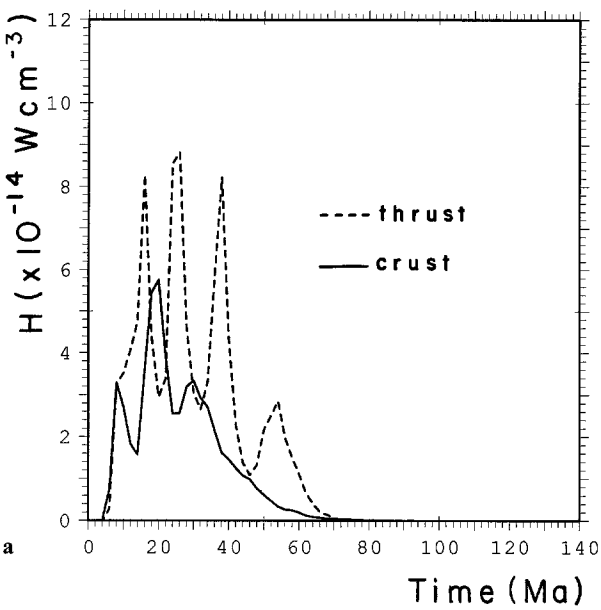

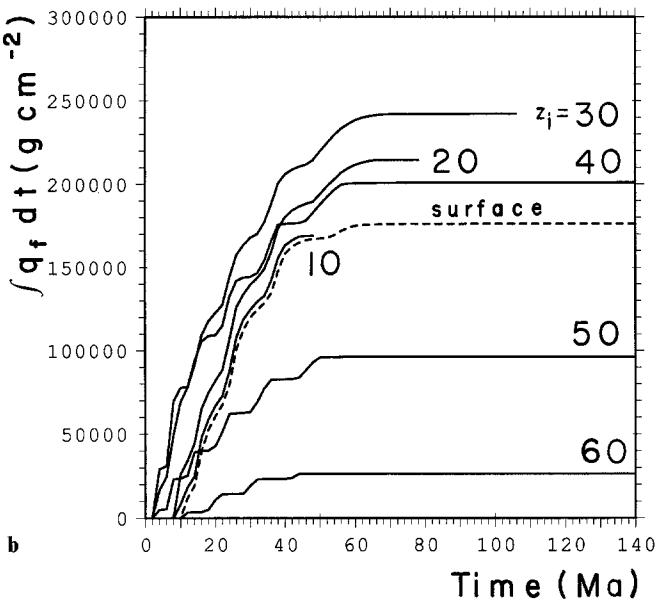

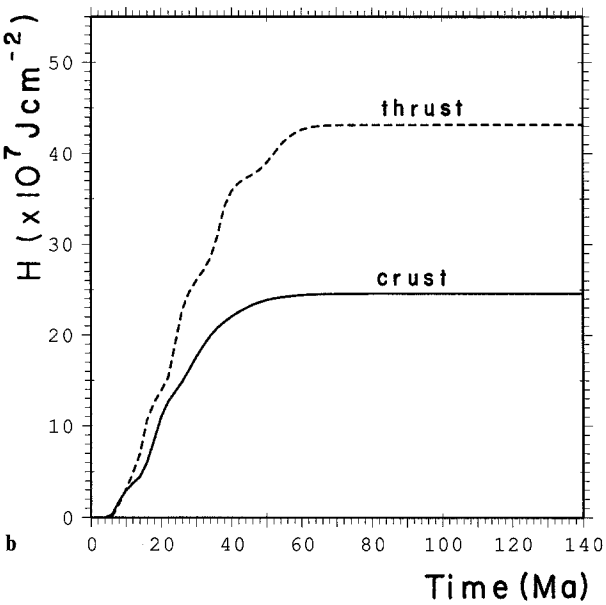

Fig. 9a, b. Time-integrated fluid fluxes through rocks at initial depths from 60 to 10 km, at 10 km intervals, for the homogeneous (**a**) and thrust (**b**) thickening models. The *dashed curves* represent the time integrated surface fluid fluxes for the two models

Fig. 10a, b. Instantaneous (**a**) and time-integrated (**b**) heat transported by fluid advection for the homogeneous (*solid lines*) and thrust (*dashed lines*) thickening models

mension, d, perpendicular to the flux, q_f. As fluid flows through this section either d or F increases. At the end of the process, the time to alter one unit volume of rock is t/d, and, if F is the volumetric ratio, the average fluid flux is:

$$q_f = F d \rho_f / t. \quad (6)$$

Given that fluid fluxes average about $5 \cdot 10^{-11}$ g/cm^2 – s for a time period in excess of 50 Ma in the rocks at initial depth of 35 km in the model crust, Eq. (6) yields a volumetric fluid-rock ratio of 500 for a rock layer with a vertical thickness of 1 m. For layer thicknesses of 100 m and 1 km, this ratio decreases to 5 and 0.5, respectively. In comparing these ratios to those obtained from petrologic studies, it must be borne in mind that the latter are usually minimum estimates based on models which maximize the efficacy of fluids as mass and heat transporters. Moreover, it is unlikely that any single petrologic fluid-rock ratio indicator is active during an entire regional metamorphic episode. In contrast to petrologic ratios, the ratios obtained from Eq. (6) are maximum estimates. Such ratios are simply a consequence of the constraint that most of the water generated during metamorphism ultimately must pass through overlying rocks to reach the surface.

Advection of heat by fluids

The instantaneous and cumulative heat transported by water in the crust is plotted in Fig. 10 for the models. Heating by fluid inflation, the fifth term in Eq. (5), is generally negligible because fluid fluxes are relatively constant with depth. Thus, fluid transported heat primarily represents the

contribution of fluid advection, the fourth term in Eq. (5), in the models. Fluid advection is a heating effect for normal geothermal gradients which increases with the magnitude of both the geothermal gradient and fluid flux. Averaged over the entire crustal thickness peak heating rates are $5.8 \cdot 10^{-14}$ W/cm^3 and $8.9 \cdot 10^{-14}$ W/cm^3 for the homogeneous thickening and thrust models, respectively, and coincide roughly with peak prograde activity. These rates are less than half the cooling rates resulting from the endothermic reactions and therefore do not have any significant effect on the overall thermal development of the models. Locally, because of the variability of time-integrated fluxes, advective heating may be slightly more important. For example, taking the average geothermal gradient to be 13 K/km, rocks at an initial depth of 30 km in the thrust model are heated by fluid advection at a rate of $6.1 \cdot 10^{-14}$ W/cm^3 for the first 60 Ma of metamorphism.

Silica transport by fluid infiltration

To evaluate the efficacy of large scale silica transport by single pass advection of metamorphic fluids, the fluids were assumed to be in equilibrium with quartz. Silica concentrations were then calculated from the equation of Fournier and Potter (1982). Fournier and Potter's equation for quartz solubilities is a fit to data obtained at pressures up to 10 kb as a function of temperature and water volume. Because the crustal models extend to depths of 70 km it was sometimes necessary to extrapolate the equation to pressures as high as 19.2 kb. The uncertainty associated with this extrapolation is likely to be negligible in comparison with that which arises due to possible variations in fluid composition. To solve the quartz solubility equation, the specific volume of water was estimated from a modified Redlich-Kwong equation of state as a function of pressure and temperature. When fluids rising upward go through the lithostatic-hydrostatic fluid pressure gradient transition the consequent expansion of the fluid results in an abrupt decrease in silica solubility. To present the best case for this mechanism for precipitating quartz, it was assumed that the lithostatic-hydrostatic transition occurs at a depth of 12 km and that silica solubility above the transition is nil.

The effectiveness of silica transport is primarily influenced by: the amount of silica consumed or precipitated when hydration/dehydration reactions take place; and the amount of silica precipitated as a result of decreasing temperature as fluids migrate upwards into cooler rocks. It is probable that most silica dissolution takes place in the rock matrix; whereas silica precipitation occurs in fluid channels. Precipitated silica should therefore be distinguishable from matrix silica, thus both the amount of quartz precipitated and dissolved are plotted as a function of depth in Fig. 11 at 10 Ma intervals. For legibility, the zero baseline of each profile in Fig. 11 is shifted 0.005 units along the quartz axes for each 10 Ma interval. Comparison of the crustal quartz profiles for the homogeneous thickening (Fig. 11a) and thrust (Fig. 11b) shows that much more silica redistribution occurs in the thrust model. This difference is due, in large part, to the lower temperature achieved in the homogeneous thickening model which lowers both silica solubility and the rate of silica solubility decrease with temperature (ds/dT). Low silica solubility reduces silica

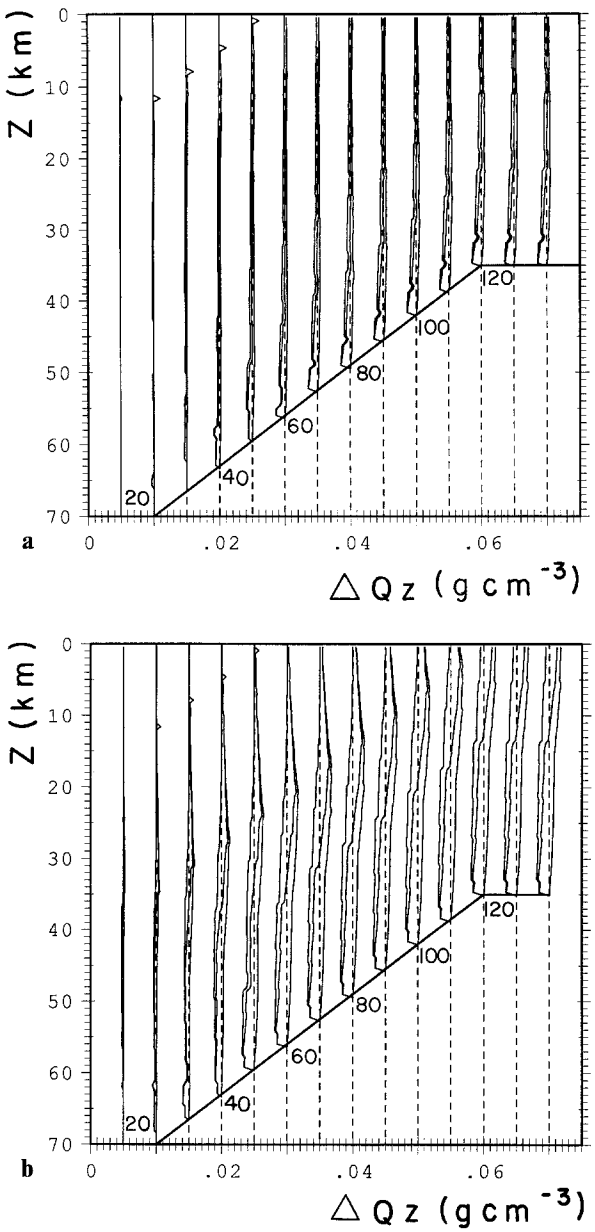

Fig. 11a, b. Crustal quartz variation profiles at 10 Ma year intervals from 0 to 140 Ma for the homogeneous (**a**) and thrust (**b**) thickening models. The zero baseline (*dashed*) for each profile is shifted by 0.005 units for every 10 Ma of model time. Alternate profiles are labelled by time in Ma. Position of the base of the crust is indicated by a *heavy solid line*. Each profile consists of three curves, the leftmost curve records the gross amount of quartz dissolution in the model, the rightmost curve records the gross amount of quartz precipitation, and the intermediate curve records the net change in quartz content

mobility and low (ds/dT) reduces the amount of silica precipitated as fluids rise through the crust.

In addition to the rate of silica solubility decrease with temperature, the amount of silica precipitated by metamorphic fluids is proportional to the time-integrated fluid flux. This flux increases upwards from nil at the base of the crust, whereas (ds/dT) is highest at the base of the crust and lowers upwards (with decreasing temperature). Thus, these effects are antithetic and combined produce a maximum in the amount of silica precipitated as a function of depth in the thrust model. This maximum is well developed

by 40 Ma in rocks at a depth of 28 km, slightly below the thrust plane, and shifts upwards at approximately the rate of erosion. The correspondence of the maximum and upper levels of the autochthonous crust is not coincidence, but is due to the upward flattening of the geotherm as it passes from radioactive autochthonous rocks into nonradioactive allocthonous rocks. This flattening leads to an unusually rapid decrease in silica solubility as fluids move upwards which favors the development of the maximum.

Intuitively it might be expected that the fluid mass transport of silica would be more important in modeling without retrograde hydration because of the higher time-integrated fluid fluxes obtained (surface time-integrated fluxes are $1.7 \cdot 10^5$ and $2.4 \cdot 10^5$ g/cm^2 for the thrust model with and without hydration reactions). However, even less silica was precipitated for the thrust model without retrograde hydration. This reflects two factors: (i) Although time-integrated fluxes are higher if retrograde hydration does not occur, the fluxes are only significantly higher in the upper, and cooler, portions of the crust where fluid silica transport is inefficient; and (ii) Silica precipitation due to retrograde water consumption is a much more effective mechanism for depositing silica than is the variation in solubility with depth. As a demonstration of this latter factor consider the amount of silica precipitated by a retrograde reaction which consumes 0.014 g H_2O per cm^3 of rock (0.5 wt %) at a depth of 27 km (7.4 kb) and a temperature of 567° C (these conditions occur in the thrust model at 60 Ma when the retrograde reaction R_4 takes place, Fig. 2b). At these conditions, silica solubility is $1.34 \cdot 10^{-2}$ SiO_2/g H_2O, and taking water density to be approximately 0.9, the reaction precipitates $1.9 \cdot 10^{-4}$ g SiO_2 per cm^3 of rock. To precipitate the same amount of silica by upward migration of a metamorphic fluid requires quite large time-integrated fluxes, the exact magnitude of which depends on the geothermal gradient. If the geothermal gradient is $15.9 \cdot 10^{-5}$ K/cm (from the thrust model geotherm in Fig. 2b at 60 Ma and 27 km), the change in silica solubility with depth is $1.35 \cdot 10^{-8}$ g SiO_2/g H_2O/cm. Thus, a time-integrated flux of 14000 g/cm^2 is required to precipitate the equivalent amount of silica ($1.9 \cdot 10^{-4}$ g SiO_2/cm^3 rock) deposited by the retrograde reaction. The present analysis ignores the actual chemistry of retrograde processes, which generally release silica (e.g., Ferry 1979; Veblen and Ferry 1983). This would enhance the effectiveness of retrograde hydration as a means of silicification.

The simulated lithostatic-hydrostatic fluid pressure transition, placed at a depth of 12 km, does not result in large accumulations of silica in any of the profiles shown in Fig. 11. This is a consequence of low silica solubilities at depths greater than 12 km, on the order of $1 \cdot 10^{-4}$ g/g H_2O, during peak prograde activity, and that, after 20 Ma, isostatic rebound continually moves the crustal column relative to the lithostatic-hydrostatic transition. If the transition is shifted to 15 km the amount of silica precipitated is about twice as large as it as 12 km; however a depth of 15 km for the transition may be considered unlikely, on rheological grounds, for most geotherms.

The maximum amount of silica procipitated in the models, about 0.003 g/cm^3 or 0.1 vol.%, is much less than the amount of vein quartz observed in many regional metamorphic terrains, which is often in excess of 1 vol.% (Yardley 1986). This discrepancy seems too large to be explained by any reasonable variation of the models or by increased silica solubility due to the electrolytes (Fournier et al. 1982) which are largely associated at high pressure. For porous media flow, the possibility that quartz is precipitated by nonequilibrium processes can be excluded because: (i) porous media flow rates are too low to result in fluid-rock thermal disequilibrium and (ii) rates of silica dissolution are high at temperatures above 300° C (Hemley et al. 1981). However, if fracture flow permits metamorphic fluids to get far from thermal equilibrium, the process of re-equilibration could precipitate large amounts of vein quartz (Yardley 1986). There are two difficulties in such a scenario. First, to get substantial thermal disequilibrium, e.g., Yardley suggests a difference of 200° C between fluid and wall-rock temperature, large fractures would be required to accommodate enormous fluid fluxes over depth intervals in excess of 15 km. Secondly, the fluid from these fractures would have to pass into an upward bifurcating fracture system to slow fluxes and permit cooling and silica precipitation. Such fracture systems are unlikely except in the upper crust. Based on this, it must be concluded that quartz veining is either a near surface (<12 km) process or that it reflects local nonhydrostatic stress or is a consequence of metamorphic reactions.

The ubiquitous occurrence of quartz and its congruent dissolution make the silica transport problem unique in that it can be treated, to a reasonable approximation, without considering the details of rock and fluid chemistry. Thus, the conclusion reached here, that one pass fluid flow is not an effective means of silica transport, cannot be generalized to include mass transport in general. In fact, to the contrary, it is likely that high electrolyte solubilities coupled with the variation in fluid-mineral partition coefficients with temperature should make the fluids generated during regional dehydration metamorphism very effective metasomatic agents.

Discussion and conclusions

The results of this study imply relatively minor roles for fluids and reaction enthalpy in the thermal budget of regional metamorphism. This conclusion is probably of general validity and supports the suggestions of England and Thompson (1984) and aspects of Peacock's (1989) work, but with regard to enthalpy, contradicts the conclusions of some earlier investigations, most notably those of Walther and Orville (1982) and Peacock (1987). It is important to realize that this difference is due to simplifications in the earlier modelling and is not an artifact resulting from different geologic assumptions.[2] The study of Walther and Orville (1982) was based on an equilibrium model which magnifies the importance of enthalpy because heat conduction was not considered. Consequently, the temperature reduction associated with devolatilization is calculated as the ratio of reaction enthalpy to rock heat capacity, roughly 100 K with Walther and Orville's parameters. Through similar arguments, Peacock (1987) suggested that retrograde hydration reactions could have a significant effect on the thermal structure of hanging wall rocks in subduction

[2] Walther and Orville assumed that a much larger quantity of fluid is released (5 wt %) than is calculated here (3 wt %). However, the fluid in Walther and Orville's model consists of 50 wt % CO_2. Thus, the enthalpy to completely devolatilise 1 cm^3 rock in their model, 0.46 kJ, is comparable to that obtained here, 0.34 kJ, and is not a major factor in the discrepancy.

zones. In reality, the effect of enthalpy is largely masked by heat conduction. Thus, the cooling effect of endothermic reactions in a metamorphic column is compensated for by increased heat flow from hotter subjacent rocks, and exothermic heating is diminished by increased heat loss to the surface. The models such as used by Walther and Orville (1982, also Yardley 1986) substantially exaggerate the rate at which heat can be supplied for devolitalization. This means that the models lead to maximum estimates for rates of fluid production and isograd advance, as well as for the enthalpy effect. This point must be borne in mind when the results of the present modelling, which is intended to refine these estimates, are compared with earlier results.

The enthalpy effect in regional metamorphism

The present modelling, and that of Peacock (1989), which takes into account thermal disequilibrium, demonstrate that even under optimal conditions the release of 2.5 to 5 wt % volatiles during regional metamorphism lowers the maximum metamorphic temperatures by less than 35 K. Peacock (1989) states that "endothermic reactions substantially retard the thermal evolution of thickened crust by as much as a factor of two in time." Although this statement would seem to belie the minor role for enthalpy suggested here, the discrepancy is largely one of definition. Peacock's statement refers to differences in the rate of advance of the 673 K isotherm in his models. This effect is particularly notable in Peacock's discontinuous reaction model because 5 wt % of volatiles are released at 673 K. The effect is primarily local and it does not, in view of the other sources of model variability, significantly alter the shape of the $P-T-t$ time paths of metamorphism.

The incorporation of retrograde effects in the models of this study is unique. Moreover, the models present the best case for retrograde effects, i.e., exothermic heating due to hydration reactions. This is because the models assume pervasive fluid flow, which is a less efficient means of releasing fluid than channelized flow. Thus, they maximize the residence time of metamorphic fluids in the crust. Despite this, the character of metamorphism is overwhelmingly endothermic, with only a short exothermic phase as the final stage of metamorphism. Heat consumption during the prograde endothermic phase averages about $6.5 \cdot 10^{-14}$ W/cm^3, and instantaneous heat consumption reaches $15 \cdot 10^{-14}$ W/cm^3 during periods of intense dehydration activity. During the retrograde exothermic phase, average heat production is on the order of $0.85 \cdot 10^{-14}$ W/cm^3 with instantaneous rates up to $2.0 \cdot 10^{-14}$ W/cm^3. Reaction enthalpy is negligible in comparison with other heat terms, such as the contributions from conductive, advective, and radioactive heating, which determine the $P-T-t$ paths followed during regional metamorphism.

Metamorphic reactions in the models only rarely control, i.e., "buffer", the local thermal state of rocks over distance intervals greater than the resolution of the models, which is about 0.5 km. In these instances, the implication that reactions locally control the metamorphic thermal environment is, perhaps, misleading because the apparent control reflects coincidental parallelism of the metamorphic geotherm with a reaction boundary. The influence of reactions is further enhanced by low rates of external heating coupled with internal heating by radioactive decay. Under these ideal circumstances, $P-T-t$ paths traced during prograde metamorphism can be reversed as paths follow a reaction boundary for time and depth intervals which may exceed 1 km and 3 Ma. Although kinetic and divariant effects result in wider isograds, both effects will lessen the influence of enthalpy on metamorphic $P-T-t$ paths.

Fluids fluxes and their consequences

Metamorphism caused by thickening of hydrated crust releases large quantities of water. Although a portion of this water is consumed by upper crustal hydration, the rocks which undergo the most extensive retrograde hydration are subsequently removed by erosion. The net result is that the post-metamorphic crust is nearly anhydrous, with 0.4–1.0 wt % water, and that almost half of the crust may consist of granulite facies rocks. The variable porosity-permeability model employed here, was used with the expectation that pore inflation during metamorphism might reduce metamorphic fluid fluxes and increase the residence time of fluids in the lower crust. However, even the conservatively low permeabilities obtained with the model, allow fluid to be drained from dehydrating rocks as fast as it is produced once the porosity reaches values between 0.4% to 0.6% (corresponding permeabilities are $1.9 \cdot 10^{-17}$ to $6.3 \cdot 10^{-17}$ cm^2). This implies, that metamorphic fluid fluxes are essentially dictated by the rate of dehydration and supports the view that lower crustal fluids are ephemeral and present only while dehydration is occurring. It must, however, be remembered that dehydration can occur along several reaction fronts over a time period of 50 to 70 Ma in response to large scale crustal thickening. Thus, the overlying rocks experience fluid fluxes between $2\text{–}7 \cdot 10^{-11}$ g/cm^2–s for a substantial time. These values are more than an order of magnitude less than the estimated maximum rate of devolitalization computed by Walther and Orville (1982, 10^{-9} g/cm^2–s) for regional metamorphism and by Peacock (1987, $3.5 \cdot 10^{-10}$ g/cm^2–s) for rocks overlying subduction zones. With more sophisticated models, Peacock (1989) obtained average fuid fluxes of $8\text{–}90 \cdot 10^{-11}$ g/cm^2–s on time scales of 40 Ma.

Over the time scale of metamorphism, even low instantaneous fluid fluxes lead to time-integrated fluxes from $2 \cdot 10^4$ g/cm^2, for high grade facies at depth, up to $2 \cdot 10^5$ g/cm^2 for shallow lower grade facies. Although, measured fluid-rock ratios cannot be directly related to fluid flux without knowledge of the natural time and distance scale of metasomatism, these fluxes appear to be more than adequate to generate the ratios obtained from petrologic studies. For example, a 1 m thick layer, containing a volumetric fluid-rock ratio indicator, subject to the maximum time-integrated flux would record a ratio of 500, whereas, under the same conditions, a 1 km thick layer would record a ratio of 0.5. Despite large time-integrated fluxes, heat advection by fluids, which averages less than $6 \cdot 10^{-14}$ W/cm^3 during prograde metamorphism, is not an important effect. Fluid channeling would have to be extremely efficient to substantially alter this conclusion, which was also reached by Peacock (1987, 1989). Lower crustal fluids also do not appear to be capable of transporting sufficient silica to explain the volume of quartz veins formed in regional metamorphic terrains, unless these veins are formed at shallow depths. More generally, however, the fluids generated in dehydration metamorphism should be highly effective in

metasomatic processes. This effectiveness should be assessed with more detailed models of fluid-rock interaction.

Isograd velocities and relict facies distributions

The thermal evolution of rocks at different depths in a collision belt is quite variable; accordingly the rates of isograd ascent through the crust also vary. In general, low grade reactions occur early in the evolution of a collision belt system when the rate of temperature change for the geotherm is greatest. This coupled with the generally high dP/dT of low grade reaction boundaries leads to maximum rates of isograd advance on the order of 10^{-10} cm/s. For high grade reactions, maximum rates of advance are up to an order of magnitude less. By way of comparison, Walther and Orville (1982) estimated the maximum rate of isograd advance to be 10^{-7} cm/s, and Peacock (1989) obtained maximum values between 10^{-8} and 10^{-9} cm/s. The rate of retrograde descent of equilibrium isograds only rarely exceeds 10^{-9} cm/s. Higher rates of retrograde descent lead to incomplete equilibration because metamorphic fluid fluxes are not adequate to furnish the water required for complete hydration.

A general feature of the $P-T-t$ paths followed during metamorphism in response to crustal thickening (England and Richardson 1977) is that the greater the initial depth of a path, then the later it will reach its maximum temperature, T_{max}. This has two implications for geothermobarometry which are well demonstrated by the facies modelling presented here: (i) Prograde reactions at depth can supply fluids which permit higher rocks to reequilibrate during cooling. In the facies models used here, this process permits low grade facies to completely reequilibrate for time periods in excess of 20 Ma after T_{max} is reached. In contrast, high grade facies cease to equilibrate almost simultaneously with T_{max}. Although only hydration/dehydration reactions are considered in the models, this result probably applies more generally to all chemical and isotopic reactions which require water as a catalyst (Rubie 1986). (ii) Regardless of whether retrograde equilibration occurs, low grade rocks will record substantially earlier conditions, i.e., cooler geotherms, than will high grade rocks. Thus, simple geothermobarometry in exhumed collision belt terrains will indicate a false geotherm which bears no relation to any geotherm of the metamorphic system (England and Richardson 1977). Retrograde equilibration reduces the time interval over which conditions are preserved and would improve the fidelity of the false geotherm.

Metamorphic porosity and variations in the hydrologic model

The conclusions of this study are based on a porous media flow model, however in real systems a variable proportion of the metamorphic fluids will be channeled in fracture systems. There is some evidence that with increasing metamorphic grade, fluid flow is less channelized even at shallow depths (Ferry 1987; Nehlig and Juteau 1988), so a porous media flow model may be realistic for the model conditions. The effect of channeling would be to reduce the fluid-rock ratios recorded in the rocks, and, perhaps, to increase the possibility of non-equilibrium fluid transfer of heat and silica. The modeling results suggest that the pattern of retrograde alteration in simple metamorphic terrains could be used to determine the dominant mode of fluid movement during metamorphism. In systems dominated by porous media flow, it is anticipated that the intensity of retrograde alteration should vary periodically with depth, whereas in fracture dominated systems a more uniform pattern should be observed. Fracture flow dominated systems would also be expected to exhibit irregular chemical and isotopic equilibration because of weak fluid-rock interaction. Some idea of the fracture density which would develop during metamorphism can be obtained by computing the characteristic compaction length (McKenzie 1985, Bickle, personal communication 1989). This length, which is proportional to the expected fracture density, will vary with the square root of permeability and, thus, will increase rapidly with porosity. Using the parameters of McKenzie (1985), together with the fluid viscosity used here and a porosity of 0.5%, a fracture density of ≈ 2.5 m is predicted.

The irregular variation of porosity within the model crust during metamorphism is largely due to the low values of permeability, proportional to the constant ω, obtained from Eq. (2). In this regard, it must be noted that even if the analytic form of Eq. (2) were not open to question, the value of ω used here yields extremely low permeabilities. Alternative porosity-permeability formulations for low porosity materials relate permeability to both higher (Ungerer et al. 1987) and lower (Bickle, personal communication 1989) powers of porosity than does Eq. (2). High order formulations would lead to less variation in the model crustal porosity, whereas lower order expressions would cause greater variation. The effect of increasing the constant ω is likewise to decrease the variation in porosity as well as the amount of the average crustal porosity. For example, if ω were increased by two orders of magnitude, then, from Eqs. (2) and (4) the porosity necessary to accommodate metamorphic fluid generation would be reduced to between 0.09 and 0.13%. An implication of this sensitivity is that extremely low steady state fluid fluxes in a crustal column characterized by a high value of ω, could generate high porosity in thin interlayers of crustal material characterized by low ω. This is intriguing because the resulting porosity variation could be a possible explanation for some deep crustal seismic attenuation (Hall 1986; Hyndman 1988; Thompson and Connolly 1989).

Limitations and extensions the modelling

The utility of this study rests largely on the degree to which its results can be relied on to provide upper limits for the production of reaction enthalpy and fluids during regional metamorphism. To some extent these results are dependent on assumed crustal water contents, dehydration enthalpies, and the location of the dehydration reactions. These are factors, which though highly variable on local scales, that are unlikely to be a major source of variation on the scale of the entire crust. A more important factor is the shape of the $P-T$ paths which result from crustal thickening. These paths are, to a great extent, determined by the thermal properties and parameters used in the models and the amount of thickening. The intensity of metamorphism is proportional to the amount of thickening. Given that the crustal thickness near continental margins is generally less than 35 km, the present models, which double the crustal thickness to 70 km, generate about the maximum amount of metamorphic heating which can be expected from a single thickening event (England and Thompson 1984, 1986).

The model thermal properties (K) and parameters (A, Q^*) are reflected in the temperature and shape of the initial geotherm. To produce the maximum amount of dehydration, the initial geotherm must be close to the low temperature limit for dehydration. This ideal is realized in the models used here, which have typical continental geotherms. Low values for A and Q^*, coupled with high K (K is proportional to quartz content), lead to cooler geotherms. However, despite the higher initial hydrate content resulting from a cooler initial geotherm, the amount of dehydration for cool geotherm models is comparable to, or less than, that generated in the models presented. This is due to the lower T_{max}, and thus less complete dehydration, of the $P-T$ paths for cool initial geotherm models. The $P-T$ paths for hotter initial geotherm models may result in virtually complete dehydration, but, because the crust initially contains less hydrate, generate less fluid. Thus, although many factors may considerably reduce the amount of enthalpy and fluid generated in the models, there are few realistic models for collision belt metamorphism which generate substantially more enthalpy and fluid than those presented here.

A possibly important limitation of this study is that effects of crustal melting are not considered. In pelitic crust, melting will probably occur either along the granite solidus, in the presence of free water, or along the muscovite + quartz decomposition curve (which corresponds approximately to the model reaction R_6 at depths greater than 20 km), for water undersaturated conditions. The $P-T$ conditions for both reactions are well within the range achieved in both the thrust and homogeneous thickening models. However, because of the rapid escape of free water from the crustal rocks, it is unlikely that much of the water released by early dehydration reactions will remain to generate large amounts of melting at the solidus. The muscovite + quartz melting reaction is potentially more important, particularly in the thrust model which results in higher metamorphic temperatures. The $P-T-t$ paths of the thrust model could generate superheated melts by this reaction in the lower 20 km of the crust. Once formed, a significant proportion of these melts could be retained long after isostatic equilibrium. These melts could therefore act as an important reservoir of both heat and water and might magnify the effect of reaction enthalpy and supply fluids to prolong retrograde activity (Connolly and Thompson 1989).

Acknowledgements. This paper benefited from reviews by Mike Bickle, George Skippen, and Doug Rumble, to whom we wish to express our gratitude. We would also like to thank Simon Peacock for providing a preprint describing a modelling study similar to that presented here. This work was made possible by computer funds from the Swiss Federal Institute of Technology and the University of Zürich. Additional support was provided by Schweizerische Nationalfonds.

References

Bear J (1972) Dynamics of fluids in porous media. American Elsevier, New York, 763 pp

Bickle MJ, McKenzie D (1987) The transport of heat and matter by fluids during metamorphism. Contrib Mineral Petrol 95:384–392

Brace WF (1984) Permeability of crystalline rocks: new in situ measurements. J Geophys Res 89:4327–4330

Connolly JAD, Thompson AB (1989) Crustal anatexis in orogenic belts. Terra Nova (in press)

Chamberlain CP, Rumble D (1989a) Thermal anomalies in a regional metamorphic terrain: an isotopic study of the role of fluids. J Petrol (in press)

Chamberlain CP, Rumble D (1989b) The influence of fluids on the thermal history of a metamorphic terrain. J Geol Soc London (in press)

Dullien FAL (1979) Porous media: fluid transport and pore structure. Academic Press, New York

England PC, Richardson SW (1977) The influence of erosion upon the mineral facies of rocks from different metamorphic environments. J Geol Soc London 134:201–213

England PC, Thompson AB (1984) Pressure-temperature-time paths of regional metamorphism I. Heat transfer during the evolution of regions of thickened continental crust. J Petrol 25:894–928

England PC, Thompson AB (1986) Some thermal and tectonic models for crustal melting in collision zones. In: Coward MP, Rice AC (eds) Collision tectonics. Geol Soc London 19:83–94

Etheridge MA, Wall VA, Vernon RH (1983) The role of the fluid phase during regional metamorphism and deformation. J Metamorph Petrol 83:205–226

Etheridge MA, Wall VA, Cox SF, Vernon RH (1984) High fluid pressures during regional metamorphism and deformation. J Geophys Res 89:4344–4358

Ferry JM (1979) Reaction mechanisms, physical conditions, and mass transfer during hydrothermal alteration of mica and feldspar in granitic rocks from south-central Maine, USA. Contrib Mineral Petrol 68:125–139

Ferry JM (1983) On the control of temperature, fluid composition, and reaction progress during metamorphism. Am J Sci 83A:201–232

Ferry JM (1986) Reaction progress: a monitor of fluid-rock interaction during metamorphism and hydrothermal events. In: Walther JV, Wood BJ (eds) Fluid-rock interactions during metamorphism. Springer, New York Berlin Heidelberg Tokyo, pp 60–88

Ferry JM (1987) Metamorphic hydrology at 13 km depth and 400–550° C. Am Mineral 72:39–58

Fisher GW (1978) Rate laws in metamorphism. Geochim Cosmochim Acta 42:1035–1050

Fournier RO, Potter RW (1982) An equation correlating the solubility of quartz in water from 25° to 900° C at pressures up to 10000 bars. Geochim Cosmochim Acta 46:1969–1973

Fournier RO, Rosenbauer RJ, Bischoff JL (1982) The solubility of quartz in aqueous sodium chloride solution at 350° C and 180 to 500 bars. Geochim Cosmochim Acta 46:1975–1978

Fyfe WS, Price NJ, Thompson AB (1978) Fluids in the earth's crust. Elsevier, Amsterdam

Graham CM, Greis KM, Sheppard SMF, Turi B (1983) Genesis and mobility of the H_2O-CO_2 fluid phase during regional greenschist and epidote amphibolite facies metamorphism. J Geol Sox London 140:577–600

Hall J (1986) The physical properties of layered rocks in deep continental crust. In: Dawson JB, Carswell DA, Hall J, Wedepohl KH (eds) The nature of the lower continental crust. Geol Soc Spec Pub 24:51–62

Hyndman RD (1988) Dipping seismic reflectors, electrically conductive zones, and trapped water in the crust over a subducting plate. J Geophys Res 93:13391–13405

Hemley JJ, Montoya JW, Marienko JW, Luce RW (1980) Equilibria in the system $Al_2O_3-SiO_2-H_2O$ and some general implications for alteration/mineralization processes. Econ Geol 75:210–228

Kirby SH (1984) Introduction and digest to the special issue on chemical effects of water on the deformation and strength of rocks. J Geophys Res 89:3991–3995

Kirby SH (1985) Rock mechanics observations pertinent to the rheology of the continental Lithosphere and the localization of shear zones. Tectonophysics 119:1–27

Lasaga AC (1986) Metamorphic reaction rate laws and development of isograds. Mineral Mag 50:359–373
McKenzie D (1985) The extraction of magma from the crust and mantle. Earth Planet Sci Lett 74:81–91
Murrell SAF (1985) Aspects of relationships between deformation and prograde metamorphism that causes the evolution of water. In: Thompson AB, Rubie DC (eds) Metamorphic reactions: kinetics, textures, and deformation. Springer, New York Berlin Heidelberg Tokyo, pp 211–241
Nehlig P, Juteau T (1988) Flow porosities, permeabilities and preliminary data on fluid inclusions and fossil thermal gradients in the crustal sequence in the central sequence of the Sumail Ophiolite (Oman). Tectonophysics 151:199–221
Peacock SM (1987) Thermal effects of metamorphic fluids in subduction zones. Geology 15:1057–1060
Peacock SM (1989) Numerical constraints on rates of metamorphism, fluid production, and fluid flux during regional metamorphism. Geol Soc Am Bull (in press)
Ridley J (1985) The effect of reaction enthalpy on the progress of a metamorphic reaction. In: Thompson AB, Rubie DC (eds) Metamorphic reactions. Springer, New York Berlin Heidelberg Tokyo, pp 80–97
Ridley J (1986) Modelling of the relations between enthalpy and the buffering of reaction progress in metamorphism. Mineral Mag 50:375–384
Ridley J, Thompson AB (1986) The role of mineral kinetics in the development of metamorphism. In: Walther JV, Wood BJ (eds) Fluid-rock interactions during metamorphism. Springer, New York, pp 154–193
Rubie DC (1986) The catalysis of mineral reactions by water and restrictions on the presence of aqueous fluid during metamorphism. Mineral Mag 50:399–415
Rumble D (1988) Fluid flow during regional metamorphism. EOS 69:465
Rutter EH, Brodie KH (1985) The permeation of water into hydrating shear zones. In: Thompson AB, Rubie DC (eds) Metamorphic reactions: kinetics, textures, and deformation. Springer, New York Berlin Heidelberg Tokyo, pp 242–250
Sibson RH (1983) Continental fault structure and the shallow earthquake source. J Geol Soc 140:741–767
Shi Y, Wang C-H (1987) Two-dimensional modeling of the P–T–t paths of regional metamorphism in simple overthrust terrains. Geology 15:1048–1051
Thompson AB (1987) Some aspects of fluid motion during metamorphism. J Geol Soc 144:309–312
Thompson AB (1988a) Dehydration melting of crustal rocks. Rend Soc Ital Min Petr 43:41–60
Thompson AB (1988b) Fluids and rock deformation. Rend Soc Ital Mineral Petrol 43:61–64
Thompson AB, Connolly JAD (1989) Metamorphic fluids and anomalous porosities in the lower crust. Tectonophysics (in press)
Thompson AB, England PC (1984) Pressure-temperature-time paths of regional metamorphism II. Their inference and interpretation using mineral assemblages in metamorphic rocks. J Petrol 25:929–955
Trimmer D (1982) Laboratory measurements of ultralow permeability of geologic materials. Rev Sci Instrum 53:1246–1254
Ungerer P, Doligez B, Chenet PY, Burrus J, Bessis F, Lafargue E, Giroir G, Heum O, Egger S (1987) A 2-D model of basin scale petroleum by two-phase flow. Application to some case studies. In: Migration of hydrocarbons in sedimentary basins. IFP Collection 45. Editions Technip, Paris, pp 415–446
Valley JW (1986) Stable isotope geochemistry of metamorphic rocks. In: Valley JW, Taylor HP Jr, O'Niel JR (eds) Stable isotopes in high temperature geological processes. Rev Mineral 16, Mineral Soc Am 445–490
Veblen DR, Ferry JM (1983) A TEM study of the biotite-chlorite reaction and comparison with petrologic observations. Am Mineral 68:1160–1168
Wall VJ, Etheridge MA (1988) Regional metamorphic fluid migration: single pass or circulation. EOS 69:464
Walther JV, Orville PM (1982) Volatile production and transport in regional metamorphism. Contrib Mineral Petrol 79:252–257
Walther JV, Wood BJ (1984) Rate and mechanism in prograde metamorphism. Contrib Mineral Petrol 88:246–259
Wood BJ, Graham CM (1986) Infiltration of aqueous fluid and high fluid: rock ratios during greenschist facies metamorphism: a discussion. J Petrol 27:751–761
Wood BJ, Walther JV (1986) Fluid flow during metamorphism and its implications for fluid-rock ratios. In: Walther JV, Wood BJ (eds) Fluid-rock interactions during metamorphism. Springer, New York Berlin Heidelberg Tokyo, pp 89–108
Yardley BWD (1986) Fluid migration and veining in the Connemara Schists, Ireland. In: Walther JV, Wood BJ (eds) Fluid-rock interactions during metamorphism. Springer, New York Berlin Heidelberg Tokyo, pp 89–108

Received October 18, 1988 / Accepted March 17, 1989
Editorial responsibility: V. Trommsdorff